

GEORGIA DOT RESEARCH PROJECT 13-28

FINAL REPORT

**Development of Guidelines for Proper Selection of Finer
Graded Aggregate Base for Georgia Pavements - Phase I**



**OFFICE OF RESEARCH
15 KENNEDY DRIVE
FOREST PARK, GA 30297**

TECHNICAL REPORT STANDARD TITLE PAGE

1. Report No.: FHWA-GA-10-1328	2. Government Accession No.:	3. Recipient's Catalog No.:
4. Title and Subtitle: Development of Guidelines for Proper Selection of Finer Graded Aggregate Base for Georgia Pavements - Phase I	5. Report Date: September 2014	
	6. Performing Organization Code:	
7. Author(s): Sung-Hee Kim and Jidong Yang (Southern Polytechnic State University)	8. Performing Organ. Report No.: 13-28	
9. Performing Organization Name and Address: Southern Polytechnic State University, Georgia Pavement and Traffic Research Center, Marietta, GA, 30060	10. Work Unit No.:	
	11. Contract or Grant No.: (RP 13-28)	
12. Sponsoring Agency Name and Address: Georgia Department of Transportation Office of Materials & Research 15 Kennedy Drive Forest Park, GA 30297-2534	13. Type of Report and Period Covered: Final; February 2014 – November 2014	
	14. Sponsoring Agency Code:	
15. Supplementary Notes: Prepared in cooperation with the U.S. Department of Transportation, Federal Highway Administration.		
16. Abstract: In this study, the effects of No. 810 screening contents in GAB on pavement performance and GAB strength were investigated. One Group I (013C) source and three Group II sources (028C, 048C, and 158C) were selected and specimens were prepared for Proctor Test, CBR measurement, and morphological analysis. It showed that Proctor and CBR test results were influenced by morphological data and particle size distribution. It was found that replacing 25% of GAB with No. 810 screening materials decreased the density and strength of Group II assemblies while the opposite was true for Group I assemblies. Pavement performance with/without screening materials in GAB was simulated using the MEPDG software based on the measured CBR. As a result, replacing GAB with 25% of screening materials increased alligator cracking when Group II sources were used and decreased alligator cracking when Group I sources were used. Nevertheless, most of the aggregate assemblies with 25% of screening materials didn't meet the GDOT's GAB gradation requirements. Thus, further investigations including the permeability, plasticity index, resilient modulus, and life cycle cost analysis, may be needed prior to the adoption of screening materials in GAB. Additionally, a new methodology was developed to estimate the stress-strain relationship of unbound aggregate base using linear viscoelastic theory. Aggregate specimens prepared from two different sources were subjected to CBR test and relaxation modulus test thereafter. From the test data, the time-dependent stress due to a known strain rate was computed as a convolution integral of the strain. The computed stress-strain relationship was compared with ones from the resilient modulus test. The results indicate that the stress-strain relationships from the resilient modulus test and the convolution integral are quite comparable with nearly same slopes when horizontal stress is assumed as approximately 45% of vertical stress. Given this agreement, the proposed methodology could be used to assist state highway agencies to validate the resilient modulus test results for quality control and quality assurance of aggregate base materials for pavement design and construction.		

17. Key Words: Aggregate, GAB, CBR, Resilient Modulus		18. Distribution Statement:	
19. Security Classification (of this report): Unclassified	20. Security Classification (of this page): Unclassified	21. Number of Pages: 56	22. Price:

Form DOT 1700.7 (8-69)

GDOT Research Project No. 13-28

Final Report

**DEVELOPMENT OF GUIDELINES FOR PROPER SELECTION OF FINER GRADED
AGGREGATE BASE FOR GEORGIA PAVEMENTS – PHASE I**

Submitted by

Sung-Hee (Sonny) Kim, Ph.D., P.E.

Associate Professor and Director
Georgia Pavement and Traffic Research Center
Southern Polytechnic State University
1100 South Marietta Parkway
Marietta, GA 30060

Jidong Yang, Ph.D., P.E.

Assistant Professor
Georgia Pavement and Traffic Research Center
Southern Polytechnic State University
1100 South Marietta Parkway
Marietta, GA 30060

Contract with

Georgia Department of Transportation

In cooperation with

U.S. Department of Transportation
Federal Highway Administration

September, 2014

The contents of this report reflect the views of the authors who are responsible for the facts and the accuracy of the data presented herein. The contents do not necessarily reflect the official views or policies of the Department of Transportation of the State of Georgia or the Federal Highway Administration. This report does not constitute a standard, specification, or regulation.

ACKNOWLEDGEMENTS

The research reported herein was sponsored by the Georgia Department of Transportation (GDOT) through Research Project No. 13-28. The financial support provided by GDOT is gratefully acknowledged. The authors would like to take this opportunity to thank Mr. Ray Coston, Ms. Gretel Sims, Mr. David Jared, and Ms. Georgene Geary at GDOT for their guidance and valuable inputs throughout the course of this project.

Table of Contents

LIST OF TABLES.....	iii
LIST OF FIGURES	iv
LIST OF ABBREVIATIONS	v
EXECUTIVE SUMMARY	viii
1.0 INTRODUCTION.....	1
2.0 OBJECTIVE	1
3.0 LITERATURE REVIEW.....	2
3.1 DEGREE OF SATURATION	2
3.2 DRY DENSITY.....	2
3.3 GRADATION AND FINE CONTENT	3
3.4 AGGREGATE TYPE AND SHAPE.....	3
4.0 LABORATORY TESTS AND RESULTS	5
4.1 MATERIAL SOURCES AND MORPHOLOGICAL PROPERTIES.....	5
4.2 PARTICLE SIZE DISTRIBUTION.....	10
4.3 PROCTOR TEST	11
4.4 CALIFORNIA BEARING RATIO (CBR) TEST	13
5.0 PAVEMENT PERFORMANCE EVALUATION	17
5.1 MEPDG SIMULATION CONDITIONS	17
5.2 GAB PERFORMANCE.....	18
6.0 DEVELOPMENT OF SIMPLE TEST METHOD TO MONITOR RESILIENT MODULUS OF GAB	21
6.1 MATERIALS AND TESTING.....	22
6.2 ANALYTICAL APPROACH FOR MODEL DEVELOPMENT	22
6.3 COMPARISON WITH RESILIENT MODULUS TEST RESULTS	29
7.0 CONCLUSIONS AND RECOMMENDATIONS	34
8.0 REFERENCES	35
APPENDIX A	
APPENDIX B	

LIST OF TABLES

TABLE	Page
4.1 Aggregate Sources and Physical Properties.....	6
4.2 Morphological Index Summary	8
4.3 Morphological Index Differences between Aggregate Groups (I and II).....	9
4.4 Morphological Index Differences across Aggregate Sources in Group II.....	9
5.1 MEPDG Inputs	17
6.1 Aggregate Types	22
6.2 AASHTO T307-99 Stress States	30

LIST OF FIGURES

FIGURE	Page
4.1 GAB Source Locations	5
4.2 Morphological Index Summary	7
4.3 Particle Size Distributions of Virgin GAB Materials	10
4.4 Particle Size Distributions of Screening Materials	11
4.5 Proctor Test Results	12
4.6 CBR Test Results	14
4.7 Gradation Changes for Group I Source	15
4.8 Gradation Changes for Group II Source	16
5.1 Evolution of Alligator Cracking: (a) 100% GAB, (b) 75% GAB/25% No. 810 screenings	18
5.2 Evolution of Permanent Deformation: (a) 100% GAB, (b) 75% GAB/25% No. 810 screenings	19
5.3 IRI Prediction: (a) 100% GAB, (b) 75% GAB/25% No. 810 screenings	20
6.1 Components of the Convolution Integral for Times Greater than t_0	24
6.2 Measured Load as Strain Is Increased Linearly and Then Held Constant	25
6.3 Relaxation Modulus Resulting from the ANN Curve Fit of Measured Stress Data Compared With the Standard Linear Solid Model With the Same Time Constant. .	28
6.4 Convolution Integral of the Curve Fit Relaxation Modulus Compared with the Measured Stress Values	29
6.5 Comparison of Measured and Calculated Stresses along with Strain.....	31
6.6 Comparison of Measured and Calculated Deviator Stresses along with Strain.....	33

LIST OF ABBREVIATION

AASHTO	American Assoc. of State Highway Officials
ANN	Artificial Neural Network
GAB	Graded Aggregate Base
GDOT	Georgia Department of Transportation
HMA	Hot Mix Asphalt
MEPDG	Mechanistic Empirical Pavement Design Guide
M_R	Resilient Modulus
NCHRP	National Cooperative Highway Research Project
NMAS	Nominal Maximum Aggregate Size
QPL	Qualified Products List
SPARC	Southern Polytechnic Applied Research Corporation
UAB	Unbound Aggregate Base
CBR	California Bearing Ratio

EXECUTIVE SUMMARY

In this study, the effects of No. 810 screening contents in GAB on pavement performance and GAB strength were investigated. One Group I (013C) source and three Group II sources (028C, 048C, and 158C) were selected and specimens were prepared for Proctor Test, CBR measurement, and morphological analysis. It showed that Proctor and CBR test results were influenced by morphological data and particle size distribution. It was found that replacing 25% of GAB with No. 810 screening materials decreased the density and strength of Group II assemblies while the opposite was true for Group I assemblies. Pavement performance with/without screening materials in GAB was simulated using the MEPDG software based on the measured CBR. As a result, replacing GAB with 25% of screening materials increased alligator cracking when Group II sources were used and decreased alligator cracking when Group I sources were used. Nevertheless, most of the aggregate assemblies with 25% of screening materials didn't meet the GDOT's GAB gradation requirements. Thus, further investigations, such as those focusing on the permeability, plasticity index, resilient modulus, and life cycle cost analysis, may be needed prior to the adoption of screening materials in GAB.

Additionally, a new methodology was developed to estimate the stress-strain relationship of unbound aggregate base using linear viscoelastic theory. Aggregate specimens prepared from two different sources were subjected to CBR test and relaxation modulus test thereafter. From the test data, the time-dependent stress due to a known strain rate was computed as a convolution integral of the strain. The computed stress-strain relationship was compared with ones from the resilient modulus test. The results indicate that the stress-strain relationships from the resilient modulus test and the convolution integral are quite comparable with nearly same slopes when horizontal stress is assumed as approximately 45% of vertical stress. Given this agreement, the proposed methodology could be used to assist state highway agencies to validate the resilient modulus test results for quality control and quality assurance of aggregate base materials for pavement design and construction.

1.0 INTRODUCTION

The ever-increasing cost of oil and gas byproducts has motivated road management agencies and the aggregate industry to pursue alternative materials and/or construction technologies to reduce the cost for pavement rehabilitation and construction. In Georgia, base materials reached a high usage of 5.7 million tons in 2007 and a low usage of 1.5 million tons in 2012. This reduction in base usage coupled with the higher demand for clean stone in asphalt and concrete materials has exacerbated the situation. As of this year, the Georgia aggregate industry has stockpiled several million tons of screening materials (No. 810 and M10), which are underutilized finer aggregates for pavement construction. Use of finer materials in the aggregate base layer has recently gained traction due to potential construction cost saving while maintaining the structural integrity of the pavement foundation. A significant cost saving would be realized if more inexpensive materials, such as No. 810 screening materials, could be used in GAB.

2.0 OBJECTIVE

The main objective of this study is to investigate the potential impacts of using No. 810 screening materials in GAB, specifically, how GAB strength and pavement performance change by varying the amount of No. 810 screening materials in the GAB layer. As a result, an acceptable percentage of No. 810 screening materials can be defined such that satisfactory mechanical properties and strength are maintained for the GAB layer.

3.0 LITERATURE REVIEW

Previous research indicates that the resilient behavior of granular materials is highly related to the degree of saturation, dry density, aggregate gradation and shape, fines content, and stress state. For mix design, it is extremely important to consider how the strength changes when those influencing factors vary in content. In this section, the effects of those factors on the strength of GAB are reviewed and discussed.

3.1 Degree of Saturation

It has been generally agreed that the degree of saturation or moisture content affects the resilient modulus of unbound aggregate base (Hicks and Monismith, 1971). Dawson (2000) studied the behavior of granular materials with high degree of saturation and found that the resilient modulus of granular materials decreases when approaching the complete saturation. When exceeding the optimum moisture content, the stiffness decreases rapidly due to the development of excess pore pressure.

Several researchers demonstrated that the effect of the degree of saturation on resilient behavior of granular materials varies by aggregate type, gradation, stress state and fine content (Hicks and Monismith, 1971, Dawson, 2000, Barksdale and Itani, 1989). Haynes and Yoder (1963) observed a 50% reduction in resilient modulus of gravel when the degree of saturation varied from 70 to 97%. Raad et al. (1992) demonstrated that the moisture content has significant effect on well graded materials with high proportion of fines because the water has better chance to be held in the pores in such gradation while the water can drain or infiltrate freely in open gradation.

3.2 Dry Density

The increase in dry density or the degree of compaction of aggregate materials makes the aggregate medium stronger and stiffer. Past research indicated that the effect of dry density or degree of compaction is a significant influencing factor for the stiffness of unbound aggregate base. The higher the dry density, the higher the resilient modulus (Kolisoja 1997). On the other hand, Thom and Brown (1987) showed that dry density has relatively insignificant effect for a crushed-limestone road base.

The effect of dry density varies by aggregate types, fine contents and stress state (Haynes and Yoder, 1963). Hicks and Monismith (1971) found that dry density plays a more important role for the partially crushed aggregates than for the fully crushed aggregates and the effect of dry density decreases as the fine content increases.

3.3 Gradation and Fine Content

A change in aggregate gradation effects a change in moisture content and dry density in GAB, thus affects the stiffness. Kim (2004) investigated the effect of gradation on resilient modulus and found that the open-graded limestone had a higher resilient modulus while no significant changes were observed for gravel.

Thom and Brown (1987) reported that the stiffness generally decreases as the fine content increases. Hicks and Monismith (1971) found that the resilient modulus decreases as fines content increases for partially crushed aggregates, but for fully crushed aggregates, the trend reverses. They also found that stiffness initially increased and then decreased as fines were added to the crushed aggregates. They argued that the initial increase in stiffness was due to the increase of the contacts as voids were filled with fines and the decrease in stiffness afterward was due to the displacement of coarse particles as excess fines were added, which results in the loss of aggregate particle interlocks and thus the load carrying capability lies only on the fines. As such, it may be inferred that the aggregate gradation and amount of fines impose an indirect effect on the stiffness of GAB by changing the moisture and density of the system. A more direct effect of gradation on the stiffness occurs when the fine particles fill the voids and influence the interaction among the coarser, angular particles. This can be visualized in the extreme situations when one compares a “floating matrix” where the coarse aggregate floats in the fines, thus preventing interaction among coarse aggregates with a lack of fines where only coarse aggregate interaction provides a resistance to movement. The optimal case lies somewhere in between, where the coarse aggregates and fine aggregates are blended in such a way to provide optimum density and maximum particle interaction.

3.4 Aggregate Type and Shape

Aggregate type and shape are significant factors influencing the resilient behavior of granular materials. The angular and rough-textured aggregates provide stronger and stiffer mass by way of

better locking, while the rounded and smooth-textured aggregates tend to slide against each other. Studies have indicated that the crushed aggregate, which typically has high angularity and rough texture, provides higher load carrying capacity and stiffness than the rounded gravel (Lekarp, 1996).

4.0 LABORATORY TESTS AND RESULTS

4.1 Material Sources and Morphological Properties

Figure 4.1 and Table 4.1 presents the sources and physical properties of selected aggregates. Two aggregate groups were studied. Group I includes one limestone source and Group II includes three granitic sources. These aggregates were selected in consultation with the GCAA and GDOT.

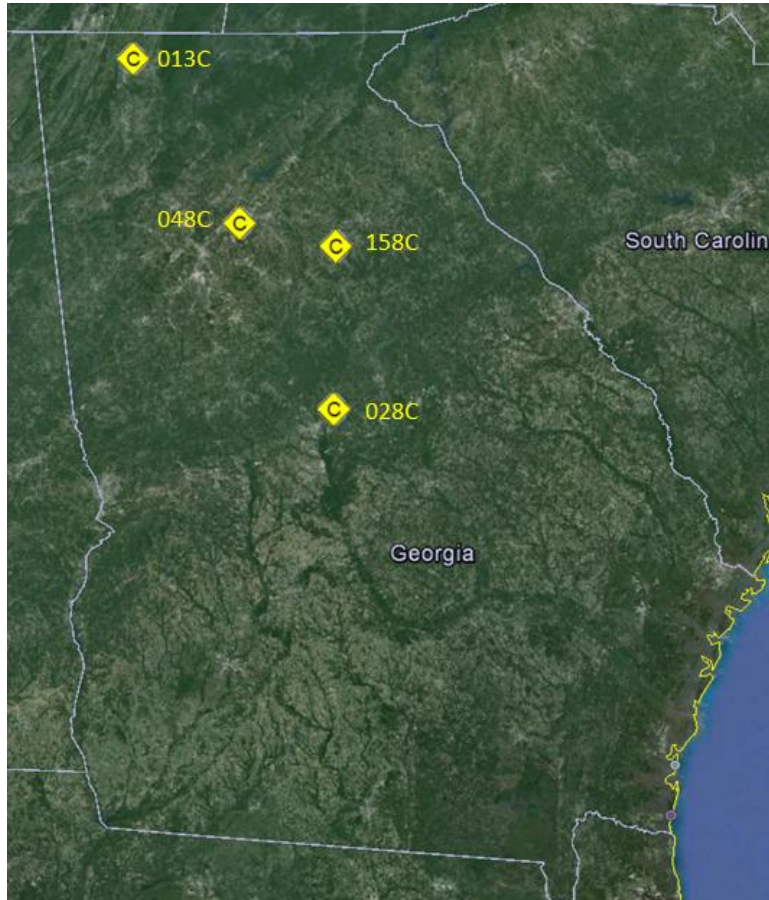


Figure 4.1 GAB Source Locations

Table 4.1 Aggregate Sources and Physical Properties

QPL ID	Aggregate Group	Source Location	GAB Character	LA Abrasion (%)	Bulk Specific Gravity
013C	I	Dalton	Limestone	25	2.702
028C	II	Hitchcock	Mylonitic Gneiss	18	2.697
048C	II	Norcross	Granite Gneiss	45	2.684
158C	II	Walton County	Biotite Gneiss	41	2.64

Besides the sources, morphological properties of mineral aggregates are known to affect pavement performance in terms of strength, modulus and permanent deformation. Current practices consider the effects of physical properties of aggregates, such as shape, texture and angularity, on the strength, stability and performance of the pavement base layer. To quantify those properties of the selected aggregate materials, the image analysis device, University of Illinois Aggregate Image Analyzer (UIAIA), was used to analyze and compute three morphological indices, i.e., angularity index (AI), flat and elongated (FE) ratio, and surface texture (ST). The UIAIA uses 3 orthogonally positioned cameras to capture 3 dimensional shape properties of aggregates. These indices are determined based on the particle image outlines obtained from each of the top, side and front views. First, aggregate samples were sieved through three sieve sizes: 19 mm, 12.5 mm, and 4.75 mm, then washed and air dried. Then, they were scanned and particle morphological indices were computed. The low bound of AI is 0, which represents a perfect sphere or no angularity, while the upper end could reach 700-800 degrees, indicating very high angularity. The ST index typically exhibits values up to 1 for smooth gravel with higher values for increasing angularity, crushed faces, corners and jagged edges in the case of 100% crushed stone (Al-Rousan et al., 2007). The morphological indices of aggregate samples are presented in Figure 4.2 and Table 4.2. As seen, the computed indices vary considerably. To distinguish the levels of difference in terms of these indices between the selected sources, hypothesis tests were conducted. The test results are summarized in Table 4.3 and Table 4.4.

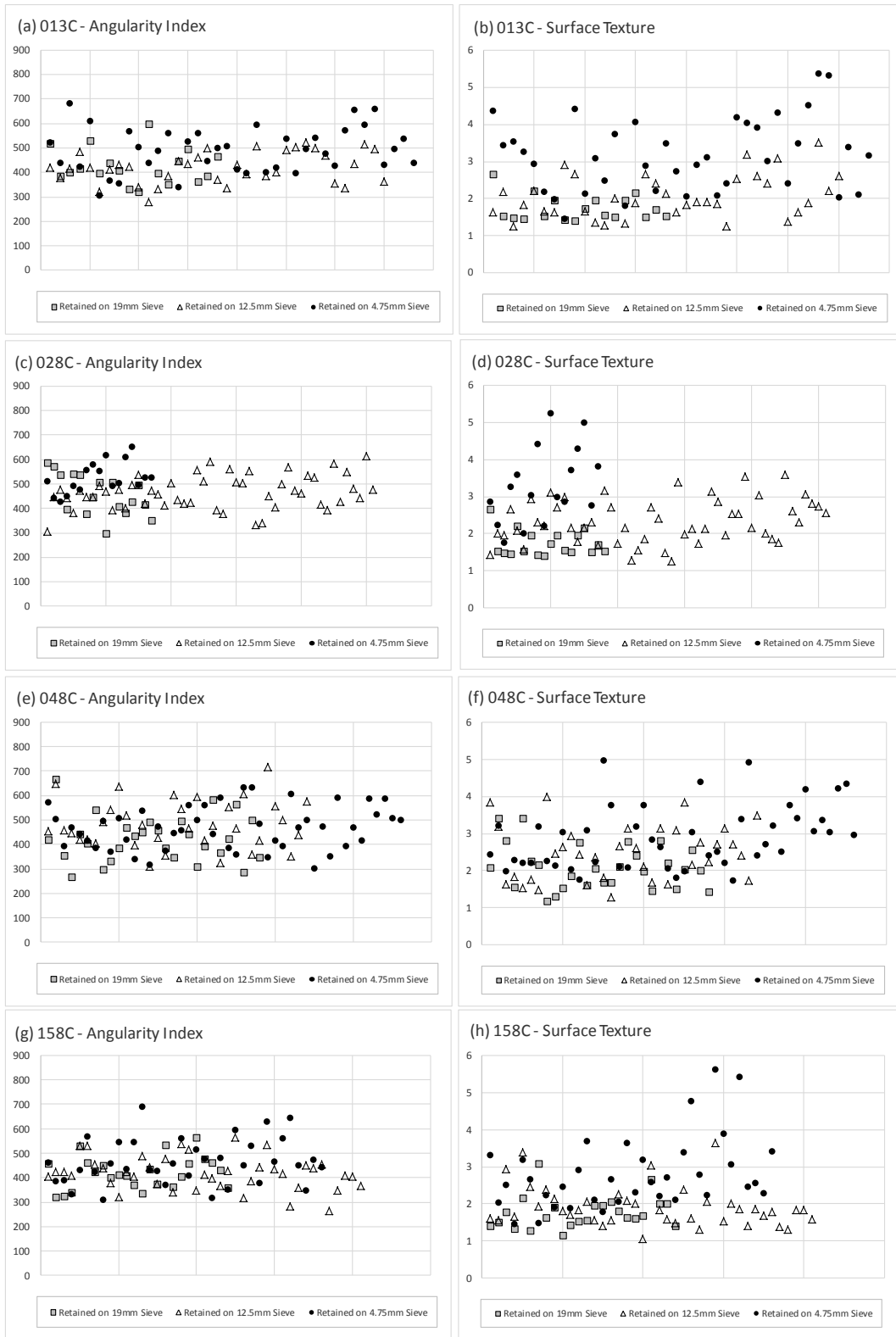


Figure 4.1 Morphological Index Summary

Table 4.2 Morphological Index Summary

Sample ID: 013C

	Retained on 19-mm			Retained on 12.5-mm			Retained on 4.75-mm		
	Angularity	FE Ratio	Surf Texture	Angularity	FE Ratio	Surf Texture	Angularity	FE Ratio	Surf Texture
Maximum	598.41	4.68	2.66	523.95	6.01	3.52	681.48	3.91	5.38
Minimum	319.46	1.52	1.40	279.25	1.88	1.26	306.54	1.39	1.46
Average	425.38	2.70	1.74	420.11	2.94	2.06	490.71	2.65	3.16
COV	16.77	32.81	19.27	15.16	32.71	27.97	18.42	25.43	30.58

Sample ID: 028C

	Angularity	FE Ratio	Surf Texture	Angularity	FE Ratio	Surf Texture	Angularity	FE Ratio	Surf Texture
Max	587.11	4.11	3.18	614.64	5.75	3.58	652.01	4.24	5.25
Min	299.19	1.86	0.97	305.22	1.36	1.26	426.25	1.85	1.76
Avg	458.34	2.91	2.18	466.04	2.88	2.33	524.89	2.62	3.30
COV	17.79	25.60	27.30	14.50	36.81	25.05	11.76	25.84	30.00

Sample ID: 048C

	Angularity	FE Ratio	Surf Texture	Angularity	FE Ratio	Surf Texture	Angularity	FE Ratio	Surf Texture
Max	667.81	5.50	3.42	716.23	5.20	3.98	635.05	4.73	4.97
Min	267.79	1.73	1.18	309.36	1.63	1.28	301.52	1.35	1.74
Avg	424.29	3.13	2.10	482.37	2.84	2.47	468.01	2.58	2.89
COV	22.02	31.74	28.04	20.09	24.02	29.43	18.50	25.82	28.90

Sample ID: 158C

	Angularity	FE Ratio	Surf Texture	Angularity	FE Ratio	Surf Texture	Angularity	FE Ratio	Surf Texture
Max	563.84	4.34	3.08	562.97	4.45	3.63	690.39	5.27	5.63
Min	322.84	1.58	1.15	262.50	1.66	1.05	310.15	1.56	1.45
Avg	421.08	2.79	1.77	418.40	2.64	1.91	465.27	2.82	2.81
COV	15.41	25.32	24.01	16.32	27.79	28.42	19.82	29.30	34.13

Table 4.3 Morphological Index Differences between Aggregate Groups (I and II)

Morphological Index	Between Sources		19 mm		12.5 mm		4.75 mm	
			t statistic	p value	t statistic	p value	t statistic	p value
Angularity	013C	028C	1.237	0.225	3.133	0.002 **	1.392	0.170
	013C	048C	-0.041	0.967	3.116	0.003 **	-1.158	0.250
	013C	158C	-0.199	0.843	-0.111	0.912	-1.182	0.241
FE ratio	013C	028C	0.733	0.469	-0.252	0.802	-0.134	0.894
	013C	048C	1.465	0.150	-0.501	0.618	-0.458	0.649
	013C	158C	0.356	0.724	-1.497	0.139	0.953	0.344
Surface Texture	013C	028C	2.628	0.013 *	2.080	0.041 *	0.470	0.640
	013C	048C	2.299	0.026 *	2.560	0.013 *	-1.346	0.182
	013C	158C	0.296	0.769	-1.157	0.251	-1.570	0.121

Notes:

* 5% significance

** 1% significance

First, the morphological indices were compared between Group I and II. In this case, 013C was compared with each of the three sources (028C, 048C, and 158C) in Group II. One-tail t test was performed to evaluate if the angularity, FE ratio, and surface texture are different between the two groups. As shown in Table 4.3. A positive t statistic value indicates a lower morphological index value of 013C comparing to other sources in Group II. As shown, for aggregates retained on 12.5 mm sieve, 013C has much lower angularity (at the 0.01 significance level) and surface texture (at the 0.05 significance level) than 028C and 048C. For aggregates retained on the 19 mm sieve, 013C also has lower surface texture (at the 0.05 significance level).

Table 4.4 Morphological Index Differences across Aggregate Sources in Group II

Morphological Index	19 mm		12.5 mm		4.75 mm	
	F statistic	p value	F statistic	p value	F statistic	p value
Angularity	1.174	0.316	7.168	0.001 **	3.197	0.045 *
FE ratio	1.050	0.356	0.893	0.412	1.081	0.343
Surface Texture	3.298	0.043 *	8.643	0.000 **	1.712	0.186

Notes:

* 5% significance

** 1% significance

Morphological indices were also compared across the sources (028C, 048C, and 158C) in Group II. For this comparison, F tests were performed. The smaller p values with asterisk indicate a rejection of the null hypothesis that the morphological indices for all three sources are

the same. As seen, for aggregates retained on the 12.5 mm sieve, significant differences were found in terms of angularity and surface texture across the sources in Group II.

4.2 Particle Size Distribution

Figure 4.3 presents the gradation of each aggregate source used in this study. Overall, the GAB gradation is much closer to the 0.45 maximum density curve representing a gradation where the aggregate particles fit together in their densest possible arrangement. It should be noted that 013C aggregate shows a drastic reduction in materials passing sieve size No. 4 compared to other sources. This implies that adding finer screening materials may create a denser mix with a gradation curve that is much closer to the 0.45 power curve. To verify this, proctor tests were conducted for each source with varying screening contents as described in next section.

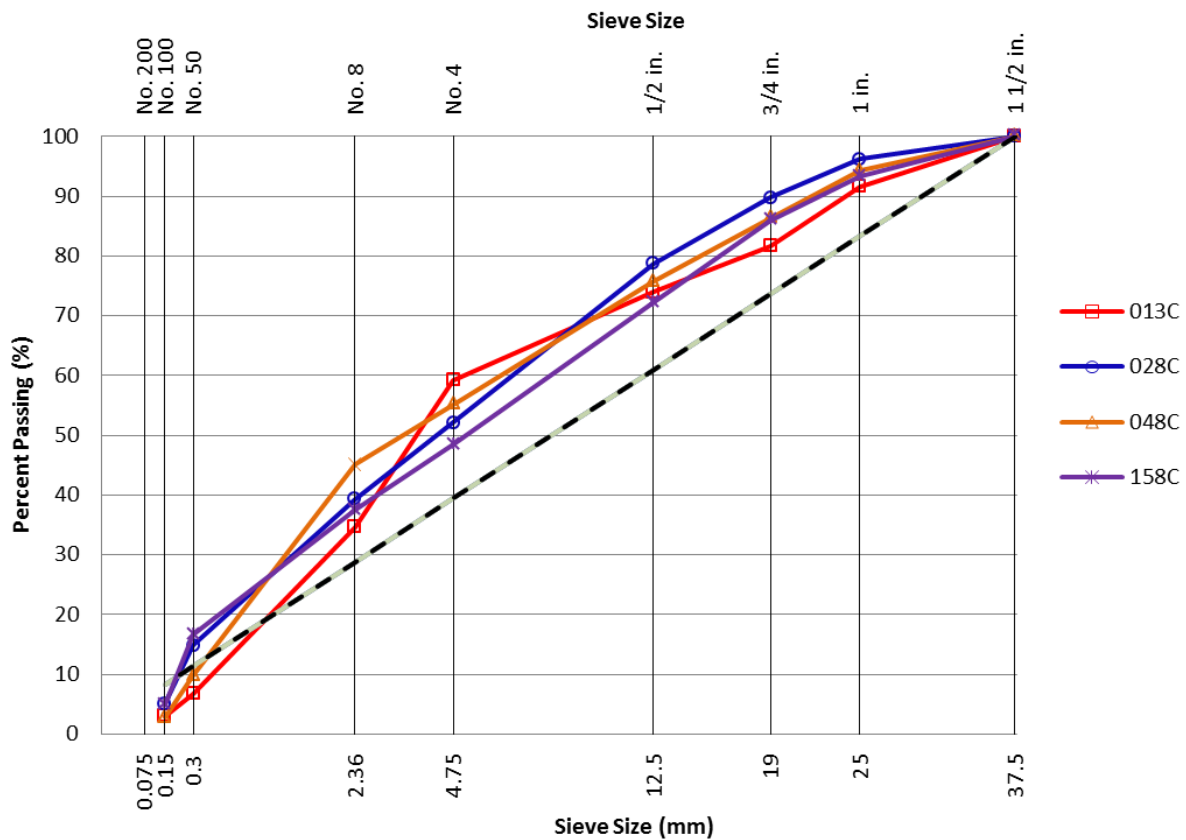


Figure 4.3 Particle Size Distributions of Virgin GAB Materials

Figure 4.4 shows the particle size distribution of No. 810 screening materials from each source. It should be noted that the 028C screening materials show relatively uniform and gap gradation with most particle sizes lying between 2.36 mm and 4.75 mm. When this type of screening material is added in GAB, it could be expected to provide aggregate interlocking to a certain degree.

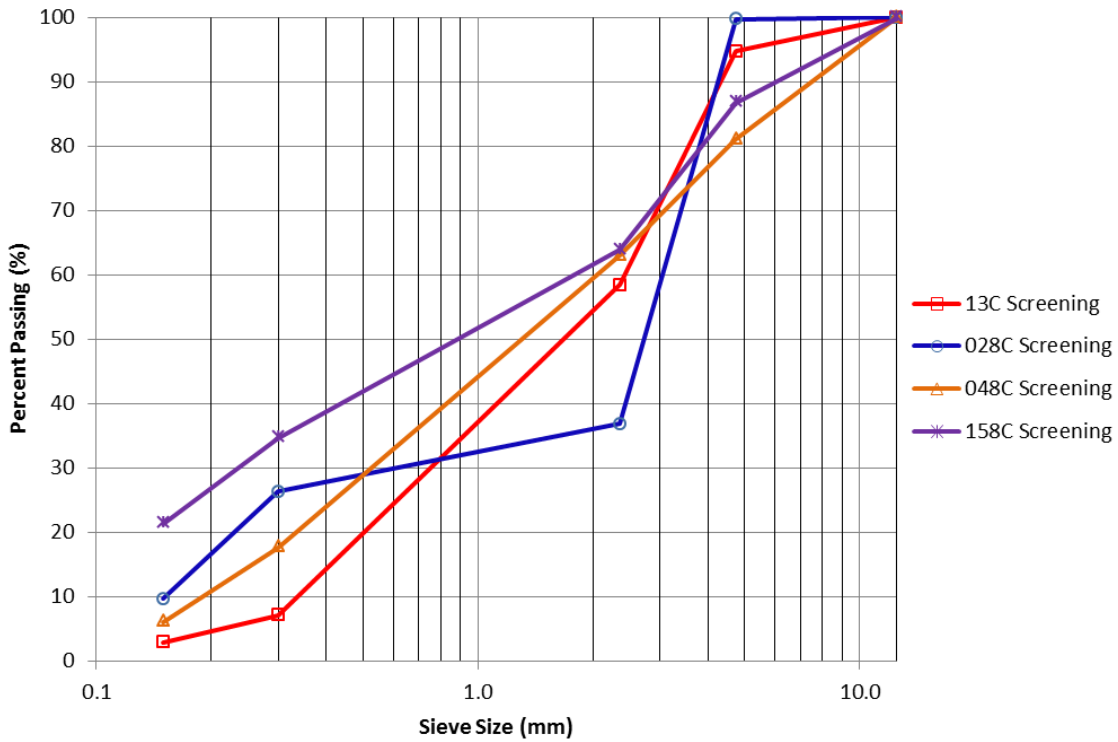


Figure 4.4 Particle Size Distributions of Screening Materials

4.3 Proctor Test

The optimum moisture content and maximum dry density were measured in conformance with ASTM D1557 using four (4) different aggregate sources prior to CBR tests. For each source of aggregates, the proctor test was conducted with varying levels of screening materials in the mix, as follows:

- 100% normal GAB
- 75% GAB with 25% 810 screenings

- 50% GAB with 50% 810 screenings

An automatic compaction apparatus was employed to perform the 56 blows per layer as prescribed by ASTM D1557. Figure 4.5 shows proctor test results.

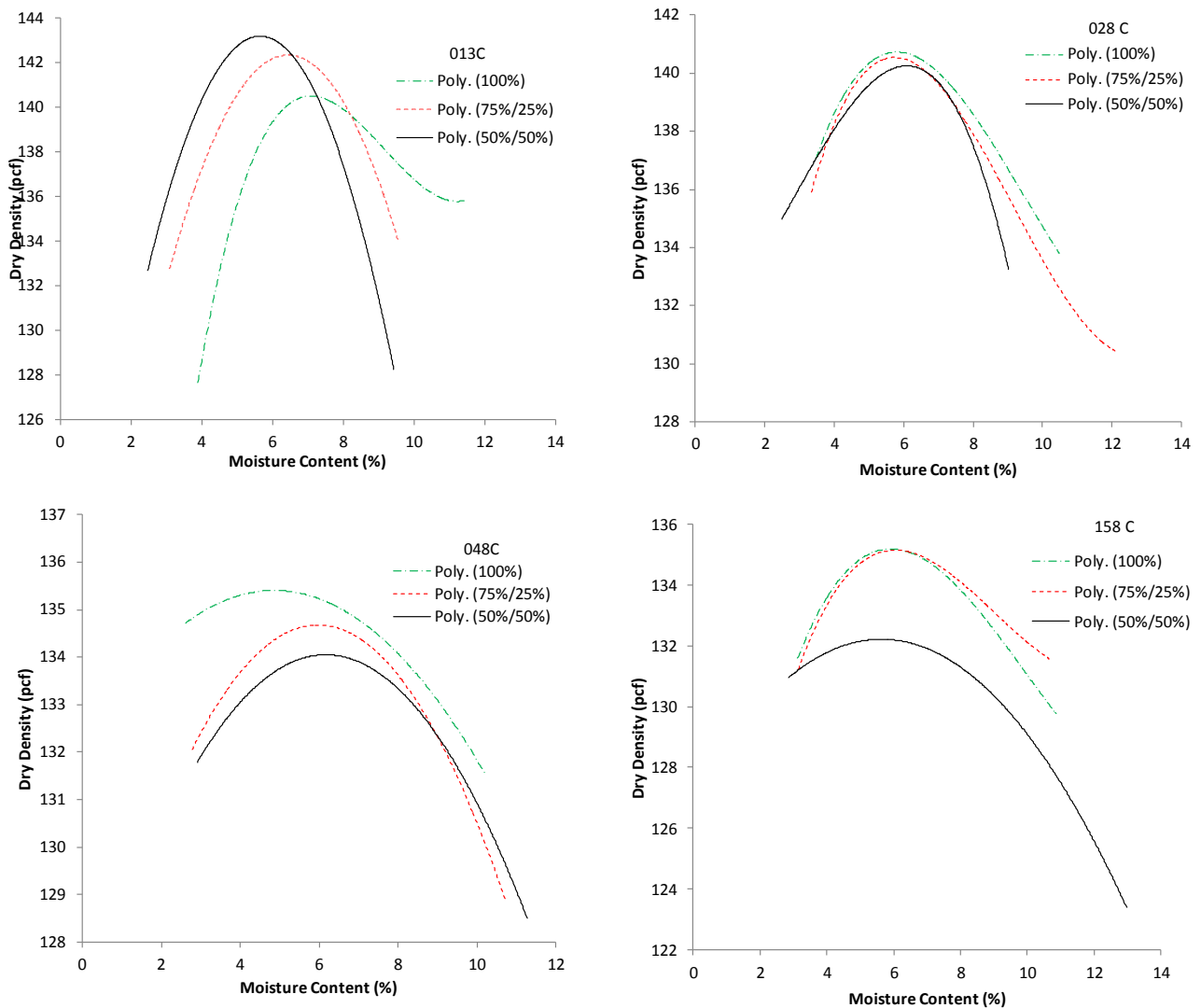


Figure 4.5 Proctor Test Results

It can be observed in Figure 4.5 that for Group I (013C) proctor curves tend to move towards the upper-left, i.e., the maximum dry density increases and the optimum moisture content decreases as the proportion of screening materials increases. This indicates that the 013C material is not completely well-graded and the finer screening particles occupy the available

voids, thereby increasing the maximum dry density. The increasing trend of the maximum dry density for 013C material is an interesting discovery because the performance of Group I aggregate could be improved by adding No. 810 screening materials.

In contrast, Group II materials (028C, 048C, 158C) all display a similar but reversing trend. The compaction curves tend to move towards the lower-right with decreasing maximum dry density and increasing optimum moisture content as the proportion of screening materials increases. This trend indicates that Group II GAB sources are well graded and adding screening materials reduces the maximum dry density. This could result in a decrease in stiffness because of the loss of aggregate particle interlocking due to excess fines being added.

4.4 California Bearing Ratio (CBR) Test

In this study, the CBR test was used to assess the quality of compacted granular materials with varying contents of screening materials. Specimens were compacted at optimum moisture with maximum dry density and subjected to CBR test in accordance with ASTM Standards D1883-05. After setting, the piston was penetrated into the specimen with a rate of 1.27 mm/min. Vertical penetration depth and load of piston were recorded. CBR value was calculated from the ratio of the vertical stress at a penetration depth of 2.5 mm and 5 mm penetration depths. Figure 4.6 summarizes the CBR test results.

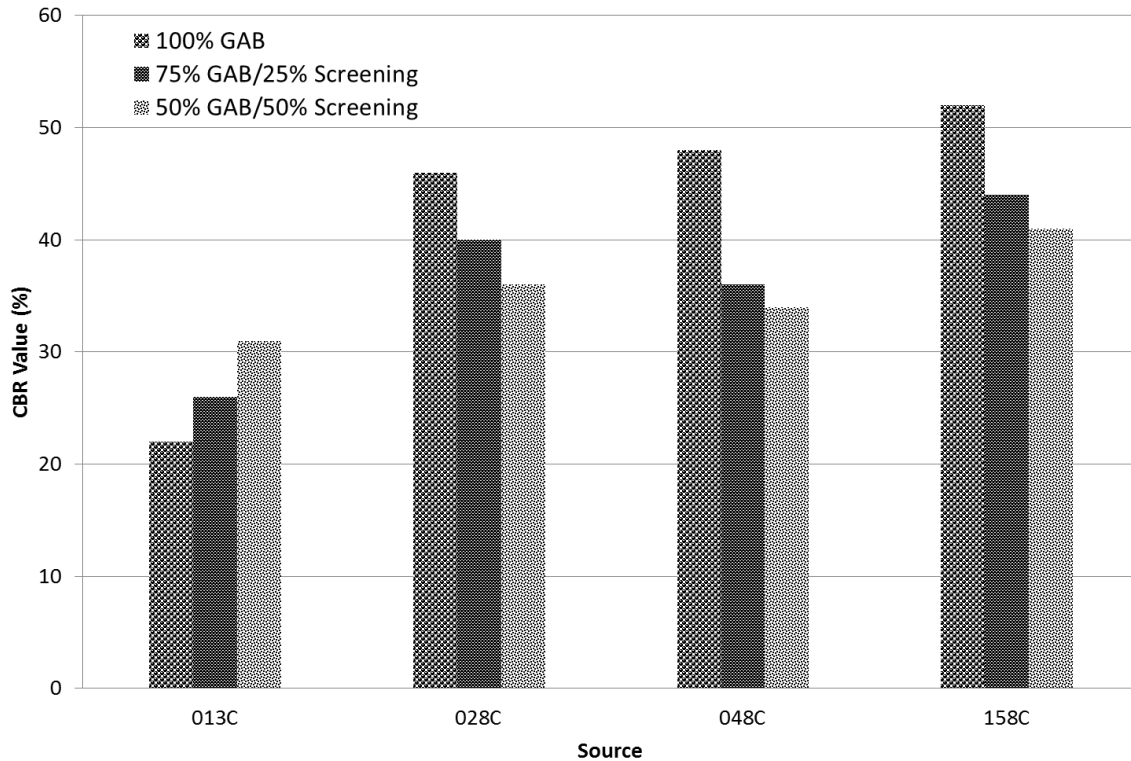


Figure 4.6 CBR Test Results

Group I (013C) shows a CBR value of 22 when 100% GAB was used, which is the lowest compared to those sources in Group II. As discussed in the previous section, angularity and surface texture of 013C were significantly lower than those of other sources. Therefore, it could be inferred that higher angularity and surface texture contribute to a stiffer GAB and thus a higher CBR value.

An interesting finding is that CBR values of the 013C source increased as more No. 810 screening materials were added. This could be due to the increased particle contacts as voids are filled by finer screening materials, resulting in increased dry density and decreased moisture content. It could also be due to the improved gradation with better aggregate interlocking provided that most particle sized of screening materials are in the range of 0.3 mm to 4.75 mm. Even though an increase of CBR was observed by increasing No. 810 screening contents, the resulting CBR values are much lower than those of other sources in Group II. Figure 4.7 illustrates gradation changes for Group I (013C) after replacing GAB with 25% and 50% screening materials. Considering GDOT's current GAB gradation requirement, it might be

possible to replace 25% of GAB with No. 810 screening materials. However, this only resulted in a marginal CBR gain of 4. As such, a benefit-cost analysis and pavement performance evaluation may be needed to identify if adding 25% screening materials is beneficial to lower the construction cost while maintaining a structurally sound pavement.

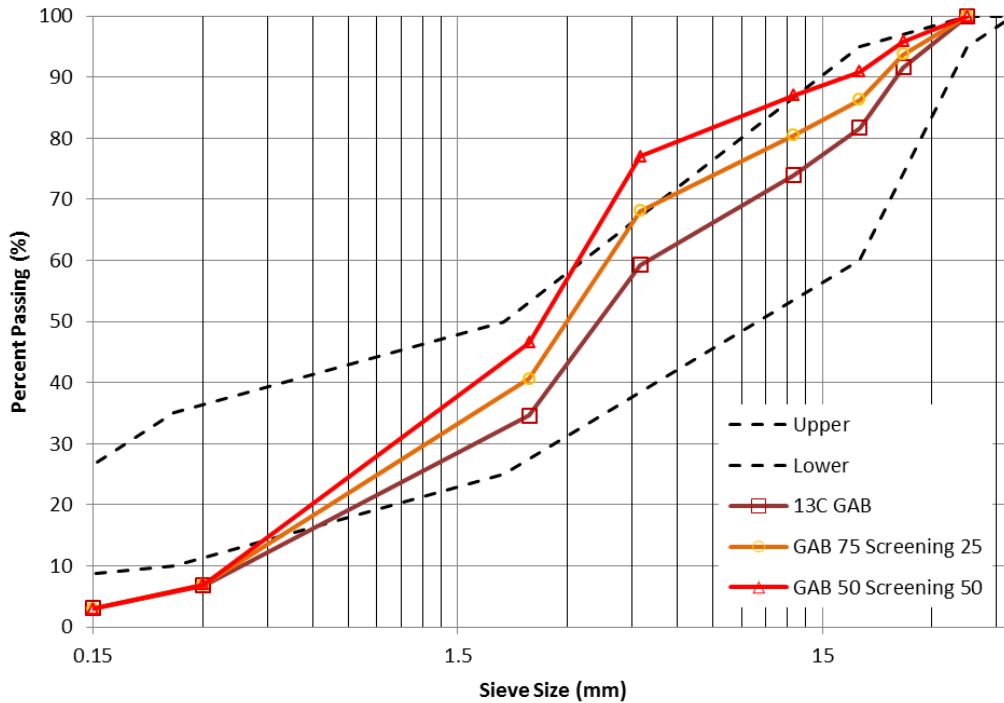


Figure 4.7 Gradation Changes for Group I Source

In comparison, CBR values for Group II (028C, 048C, 158C) sources are higher and in the range of 46 to 53 when 100% GAB was used. A decreasing trend in CBR was observed for all Group II sources as more GAB was replaced by the screening materials. This may imply that the gradations of Group II GAB sources were already well graded and adding more fines could result in a loss of interlocking among aggregates. The level of decrease in CBR varied depending on aggregate sources and grading. In particular, 048C source experiences the largest drop in CBR as the screening materials were added. Figure 4.8 shows the gradation changes for Group II sources when the original GAB is replaced by 25% screening materials. As shown in Figure 4.8, replacing 25% GAB with screening materials results in gradation curves exceeding the upper limit of GDOT's GAB gradation requirement.

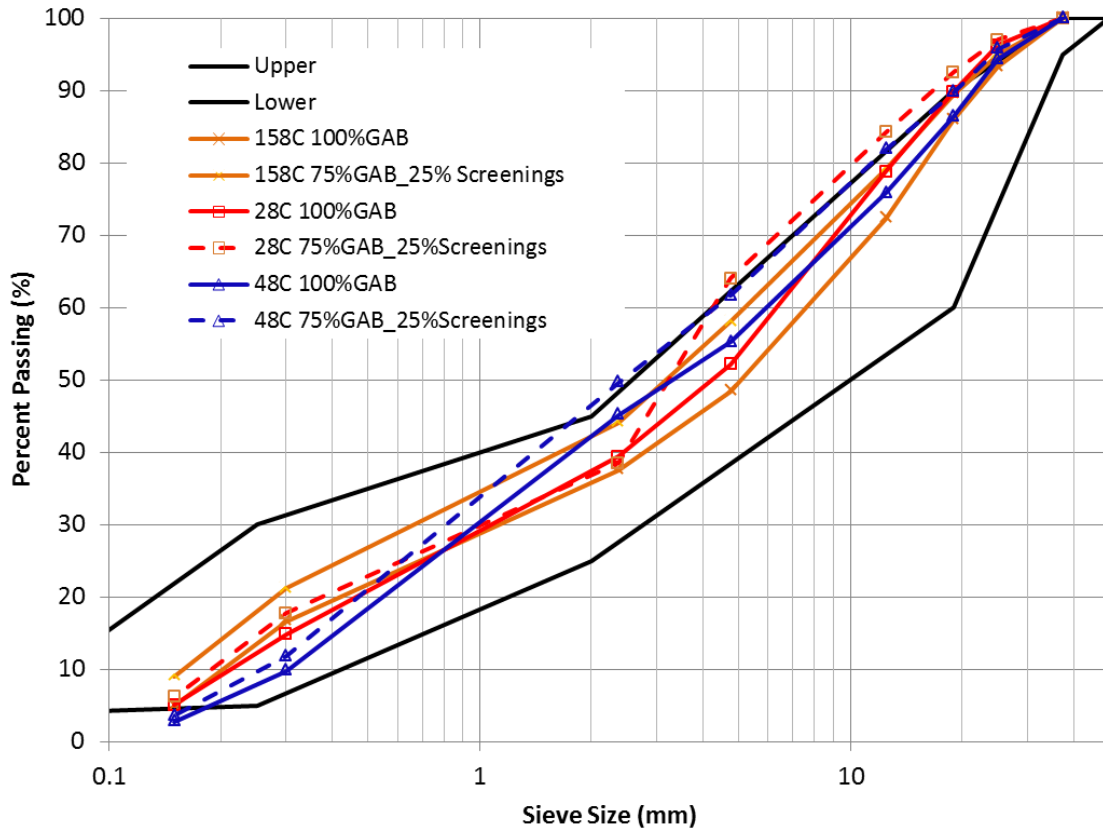


Figure 4.8 Gradation Changes for Group II Source

5.0 PAVEMENT PERFORMANCE EVALUATION

5.1 MEPDG Simulation Conditions

The design of the aggregate base layer, which is a constitutive component of pavement structure, would be better evaluated by way of the overall pavement performance. For this evaluation, SR 17/US78 project was utilized as a test section (Introduction to AASHTOWare Pavement ME Design for Georgia DOT, August 2013). Mechanistic Empirical Pavement Design Guide (MEPDG) program Version 1.10 was used . For more accurate and rigorous comparison, design parameters for SR17/US78 Pavement Reconstruction Project in McDuffie/Wilkes County were utilized as summarized in Table 5.1.

Table 5.1 MEPDG Inputs

Traffic Data	<ul style="list-style-type: none"> • 2018 Average Daily Traffic, one-way or direction: 3,500 • 2038 Average Daily Traffic, one-way or direction: 5,300 • Lane Distribution factor: 0.90 • 2018 Average Annual Daily Truck Traffic: 781 (this value represents 22 percent trucks based on an AADT of 3,500. • Average Annual Growth Rate of Trucks (%): 2.6 percent; assumed to be the same as AADT • Design 18 KESALS; Cumulative over Design: 5,701,300
Structure	<ul style="list-style-type: none"> • 1.5” SMA • 2” HMA with PG 64-22 • 4” HMA with PG 64-22 • 12” Non-stabilized Base
Materials Inputs	<ul style="list-style-type: none"> • HMA E* - GDOT RP 12-07 Report • GAB CBR was measured in this study. • Soil : 2’ Silty Clay/2’ Clayey Silt/4’ Silty Clay • Soil support value of 3.5

A three layer asphalt pavement structure was considered for this study. The asphalt structures for the MEPDG simulations were composed of a 7.5-inch HMA, a 12-inch Aggregate Base, and subgrade, detailed in Table 5.1. Specifically, HMA E* values were obtained from GDOT RP 12-07 database and GAB CBR values were obtained from the current study. Two design alternatives for the aggregate base layer, (1) 100% GAB, and (2) 75% GAB/25% screening materials, were evaluated.

5.2 GAB Performance

In MEPDG simulations, alligator cracking, permanent deformation, and IRI were estimated based on the inputs in Table 5.1. Figure 5.1 shows the evolution of alligator cracking. Except for the GAB layer, other layers' inputs remained the same. Level 2 CBR values were entered in Pavement ME depending on the screening contents as shown in Figure 4.6.

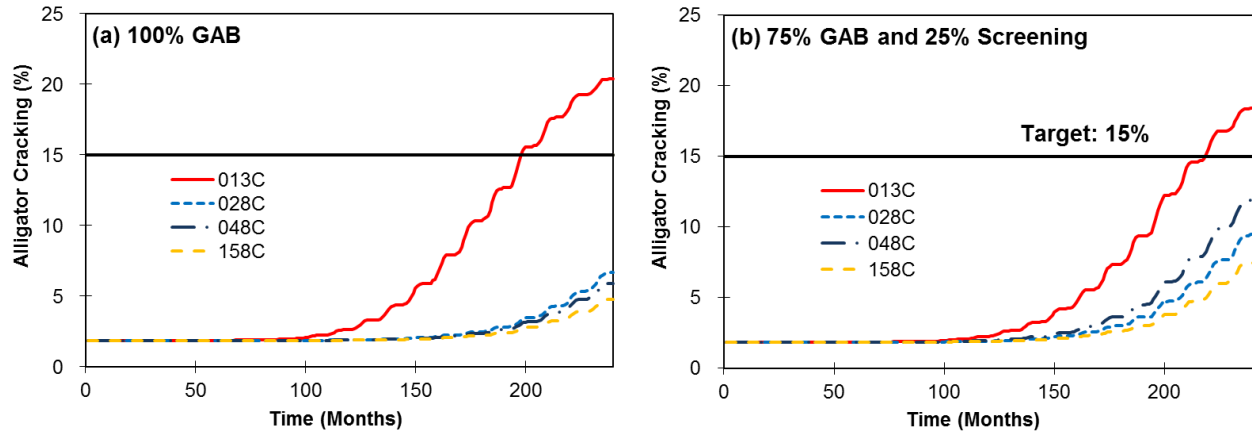


Figure 5.1 Evolution of Alligator Cracking: (a) 100% GAB, (b) 75% GAB/25% No. 810 screenings

The upper limit of vertical axis (y-axis) represents the design limit value of each performance index. The design limit for alligator cracking was set as 15%, which is commonly used in Georgia. In Figure 5.1, alligator cracking was predicted to exceed the failure criterion for 013C source. In contrast, when 25% of GAB was replaced with No. 810 screening materials, alligator cracking was reduced to 18%. As such, it could be inferred that replacing 25% of 013C GAB with No. 810 screening materials would increase the stiffness of GAB layer and improve pavement performance by reducing alligator cracking although it is still above the design limit. For Group II sources, alligator cracking was predicted to not exceed the failure criterion for both 100% GAB and 75% GAB with 25% of screening materials. However, alligator cracking increased significantly when GAB was replaced by 25% of screening materials. Since Group II sources with 25% of screening materials increase alligator cracking up to 50% and exceeded the upper limit of GDOT's GAB gradation requirement, further investigations may be needed prior to the adoption of screening materials in the GAB layer.

Figure 5.35.2 shows the total rut depths of the pavement structures simulated. There appears to be little performance difference in rut depth between the two design alternatives because the trends of evolution are quite similar and overlapping each other. For a 20-year simulation, the rut depths were predicted to be lower than the design limit of 0.5 inch. Therefore, one could conclude that use of screening materials up to 25% of GAB would likely not result in significant performance difference in terms of permanent deformation.

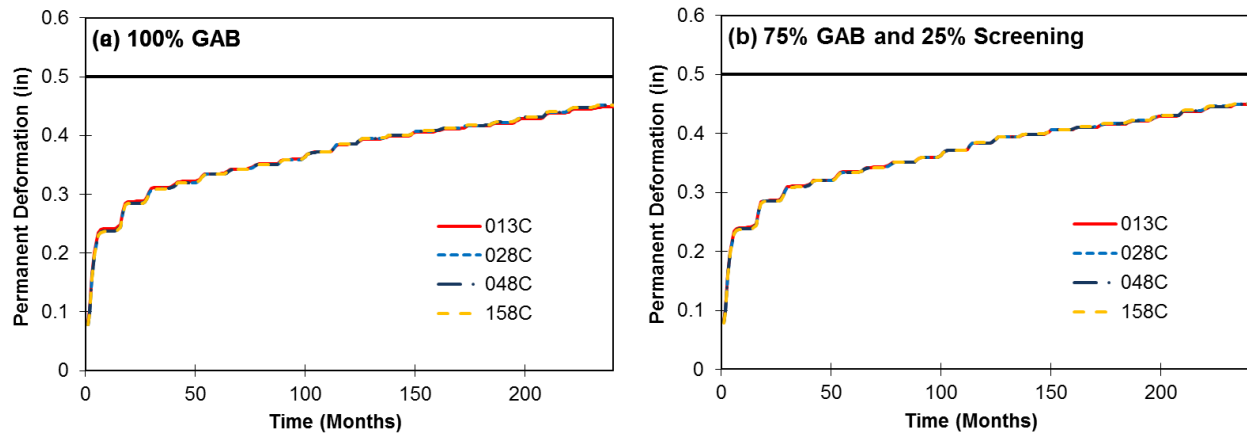


Figure 5.2 Evolution of Permanent Deformation: (a) 100% GAB, (b) 75% GAB /25% No. 810 screenings

International roughness index, IRI, has been used to measure road roughness for evaluating and managing road systems. IRI is calculated based on the longitudinal profiles of wheel paths and is a function of pavement distresses, including fatigue and thermal cracking. Figure 5.2 illustrates IRI progression over time. As shown, IRI trends associated with different source materials converge and little difference was found between the two alternatives: 100% GAB and 75% GAB/25% Screenings. Therefore, it may be concluded that the aggregate types and 25% GAB replacement with screening materials would not likely affect a difference in the performance of asphalt pavements in terms of IRI.

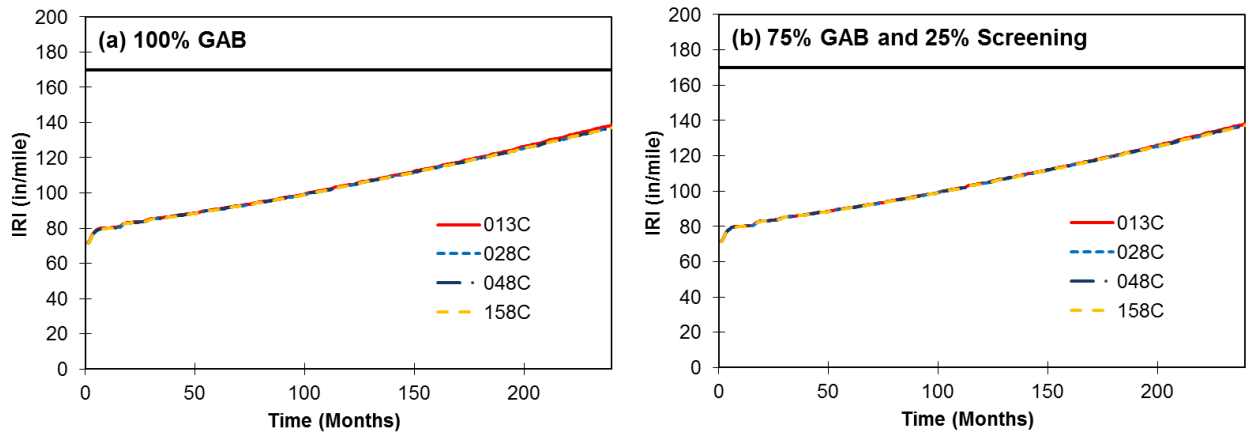


Figure 5.3 IRI Prediction: (a) 100% GAB, (b) 75% GAB /25% No. 810 screenings

6.0 DEVELOPMENT OF SIMPLE TEST METHOD TO MONITOR RESILIENT MODULUS OF GAB

The characterization of load-deformation behavior of unbound granular materials is extremely important for the design of a reliable unbound pavement foundation. In 1993, the American Association of State Highway and Transportation Officials (AASHTO) proposed a pavement design procedure using the resilient modulus (M_R) concept to describe the behavior of pavement materials under surface traffic loadings. The M_R is defined as the ratio of applied dynamic deviatoric stress to the resilient strain.

The current Pavement ME design approach adopted resilient modulus concept to consider nonlinear and stress-dependent behavior of unbound granular materials under repeated wheel loading conditions. Characterizing the resilient behavior of aggregate bases in terms of stress-dependent resilient modulus is commonly done using cycle load triaxial tests. The resilient behavior of the aggregate systems is then characterized based on Mechanistic-Empirical Pavement Design Guide (MEPDG) model in Eq.(1).

$$M_R = k_1 \left(\frac{\theta}{P_a} \right)^{k_2} \left(\frac{\tau_{oct}}{P_a} + 1 \right)^{k_3} \quad (1)$$

where:

M_R = resilient modulus (kPa),

θ = the bulk stress (kPa),

τ_{oct} = octahedral shear stress (kPa),

P_a = atmospheric pressure (kPa), and

k -values = material coefficients

The determination of material coefficients through repeated load triaxial test is important for accurate prediction of the resilient behavior of granular materials which is a direct input for reliable pavement design. Such tests, however, are considered to be too expensive to implement in routine road construction and design projects. To simplify the method of estimating resilient material coefficients, there have been several attempts aiming to correlate aggregate physical properties with resilient properties based on regression techniques (Kim et al., 2007, Xiao et al., 2011). However, these regression relationships are valid only for the materials used in

developing the models. In this regard, a simple methodology is needed to model stress-strain relationship based on mechanistic principles, which can be used to predict the resilient behavior of aggregate bases. In this paper, a new methodology to model stress-strain relationship of unbound granular bases is proposed based on experimentally determined relaxation modulus using CBR equipment and mechanical principles.

6.1 Materials and Testing

Table 1 shows the two aggregate sources selected to determine resilient behavior. Fig. 1 shows the gradation of each aggregate source used in this study.

Table 6.1 Aggregate Types

Material ID	Aggregate Group	Source Location	GAB Character	LA Abrasion (%)	Optimum Moisture Content (%)	Max. Dry Density (pcf)	Bulk Specific Gravity
013C	I	Dalton	Limestone	25	6.6	142.5	2.702
028C	II	Hitchcock	Mylonitic Gneiss	18	6.2	141.2	2.697

Note: 1 pcf = 16.02 kg/m³

6.2 Analytical Approach for Model Development

The relaxation modulus is defined by the ratio of the time variation of stress $\sigma(t)$ and a step strain ε_0 at a fixed temperature in Eq. (2).

$$E(t) = \frac{\sigma(t)}{\varepsilon_0} \quad (2)$$

CBR equipment is obviously incapable of instantaneously applying a step strain, but can linearly ramp up the strain and hold it constant after completion of the CBR test. Inducing the relaxation modulus from measured stresses in such a situation requires writing the stress/strain relationship as a convolution integral.

A small strain $\Delta\varepsilon_1$ applied at time τ_1 and held would produce a stress of

$$\sigma(t) = E(t - \tau)\Delta\varepsilon \text{ for } t > \tau \quad (3)$$

Assuming that the relation between applied strain and stress is linear, the response to a series of small strains applied at constant time intervals would be described as Eq. (4) by the superposition principle.

$$\sigma(t) = \sum \sigma_i = \sum E(t - \tau_i)\Delta\varepsilon_i \quad (4)$$

It should be also worth to note that stress and strain results from the relaxation modulus test in this paper are actually pseudo stress (force applied by the plunger divided by the plunger area) and pseudo strain (down movement of the plunger divided by the height of the sample).

The summation in Eq. (4) reduces to the continuous distribution

$$\sigma(t) = \int_0^t E(t - \tau)d\varepsilon = \int_0^t E(t - \tau) \frac{d\varepsilon(\tau)}{d\tau} d\tau = \int_0^t E(t - \tau)\dot{\varepsilon}(\tau)d\tau \quad (5)$$

in the limit as $\Delta\varepsilon$ approaches zero, which is modified using the chain rule since strain ε varies in time. Eq. (5) represents the convolution of relaxation modulus and strain rate, which can be rewritten as

$$\sigma(t) = \int_0^t E(\tau)\dot{\varepsilon}(t - \tau)d\tau \quad (6)$$

due to the commutative property of convolution.

Eq. (6) can be modified to reflect the average relaxation modulus

$$\frac{\sigma(t)}{\dot{\varepsilon}t} = \frac{1}{t} \int_0^t E(\tau)d\tau = \bar{E} \text{ for } t < t_0 \quad (7)$$

when strain is ramped up at a constant strain rate $\dot{\varepsilon}$ until time t_0 after which strain is held constant. The CBR test equipment collects stress data at sampling frequency f where each sample is taken at intervals of $\Delta t = 1/f$. The stress acquired during the n^{th} interval is denoted σ_n where

$$\frac{\sigma(t)}{\dot{\varepsilon}n\Delta t} = \frac{\sigma(n\Delta t)}{\dot{\varepsilon}n\Delta t} = \frac{1}{n\Delta t} \int_0^{n\Delta t} E(\tau)d\tau = \bar{E}_{0,n} \text{ for } n\Delta t < t_0 \quad (8)$$

with $\bar{E}_{i,j}$ representing the average relaxation modulus during the interval $i\Delta t \leq t < j\Delta t$. The average relaxation modulus can also be written as

$$\bar{E}_{0,n} = \frac{(n-1)\bar{E}_{0,n-1} + E_n}{n} \quad (9)$$

where E_n is the average during interval n , which approximates the value $E(n\Delta t)$ for small Δt . Combining Eqs. (8) and (9) and rearranging, the average relaxation modulus during any time interval up to $n_0 = t_0/\Delta t$ can be expressed as

$$E_n = \frac{n\sigma_n - (n-1)\sigma_{n-1}}{\varepsilon n \Delta t} \text{ for } n \leq n_0 \quad (10)$$

which depends only on the stress measurements, sampling rate, and strain rate. Time constants for relaxation moduli generally fall in the range of minutes or longer so averages over fractions of seconds with modern digital acquisition systems produce more than adequate time resolution.

Developing an expression of relaxation modulus for times greater than t_0 , i.e. after strain ramping is complete, is slightly more complicated. The convolution of E and $\dot{\varepsilon}$ in Eq. (6) captures information about E only over the last t_0 , as illustrated in Figure 6.1, resulting in

$$\frac{\sigma_n}{\varepsilon t_0} = \frac{1}{t_0} \int_{t-t_0}^t E(\tau) d\tau = \bar{E}_{n-n_0+1,n} \text{ for } t > t_0 \quad (11)$$

Combining this with

$$\bar{E}_{n-n_0+1,n} = \frac{E_n + (n_0-1)\bar{E}_{n-n_0+1,n-1}}{n_0} \quad (12)$$

generates the recursive expression

$$E_n = \frac{\sigma_n - \sigma_{n-1}}{\varepsilon \Delta t} + E_{n-n_0-1} \text{ for } n > n_0 \quad (13)$$

whose base case is Eqn. (10).

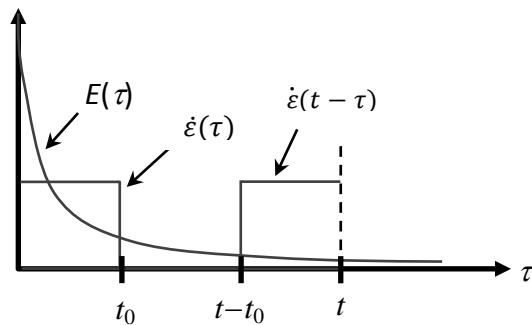


Figure 6.1 Components of the Convolution Integral for Times Greater Than t_0 .

Eqs. (10) and (13) are valid as long as the material is experiencing linear behavior during the non-zero portion of the convolution integral. Unfortunately, the aggregate material supports essentially no load when strain is first applied as the empty spaces between the aggregate are closed, as appears for small times in Figure 6.2. Such nonlinear stress-strain behavior unfortunately skews the results at all subsequent times due to the recursive nature of Eqs. (10) and (13). In order to overcome this problem, a curve fit is generated for the relaxation modulus using only Eq. (13), i.e. with data acquired after strain is held constant. This time is chosen because Eq. (13) still captures information about E at all times since $E(0)$ is covered by $\dot{\epsilon}(t - \tau)$ when $t=t_0$ in Figure 6.1. Additionally, solving for an E satisfying the convolution integral with data starting when strain is held constant seeks to eliminate any effects from not applying an instantaneous strain impulse as defined in Eq. (2).

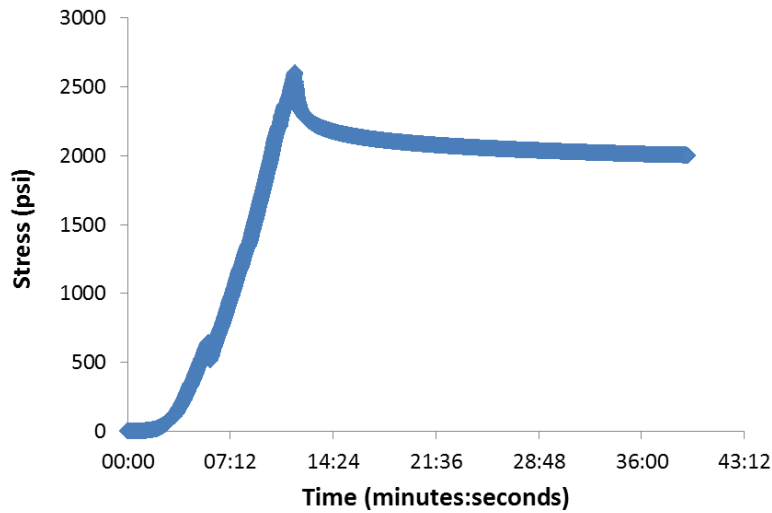


Figure 6.2 Measured Load as Strain Is Increased Linearly and Then Held Constant.

In fact, if the material were to follow any of the well-known exponentially decaying models such as the Burgers or Standard Linear Solid Model (Findley, Lai, Onaran, 1976), the effect of a ramped rather than instantaneous strain application results in a simple time delay in the relaxation modulus. For example, consider the exponential relaxation modulus

$$E_{\text{exp}} = Ae^{-t/B} \quad (14)$$

Inserting Eq. (14) into the convolution integral in Eqn. (6) for times t greater than t_0 for a strain ramped at rate $\dot{\epsilon}$ gives

$$\sigma(t) = \dot{\epsilon} \int_{t-t_0}^t A e^{-\tau/B} d\tau = \dot{\epsilon} t_0 A \frac{B}{t_0} (e^{t_0/B} - 1) e^{-t/B} = \dot{\epsilon} t_0 A e^{-(t-t_d)/B} \quad (15)$$

where $\dot{\epsilon} t_0$ is the value of strain held constant after t_0 , and

$$t_d = B \ln \left[\frac{B}{t_0} (e^{t_0/B} - 1) \right] \quad (16)$$

is a constant dependent on the ramp time t_0 and the decay coefficient B . The apparent relaxation modulus

$$\frac{\sigma(t)}{\dot{\epsilon} t_0} = A e^{-(t-t_d)/B} \quad (17)$$

implied by Eq. (15) obtained by a ramped rather than instantaneous strain is simply the exponentially decreasing relaxation modulus in Eq. (14) delayed by t_d . It can be similarly shown that relaxation moduli which are linear combinations of exponential, linear, or constant terms will exhibit time-delayed responses to ramped strains as well.

Rather than assuming the material obeys a familiar model, a non-linear curve fit with the sum squared error function

$$S = \sum_{n=n_0+2}^M \left(E_n - E_{n-n_0-1} + \frac{\sigma_{n-1} - \sigma_n}{\dot{\epsilon} \Delta t} \right)^2 = \sum_{n=n_0+2}^M G_n^2 \quad (18)$$

based on Eq. (13) is performed to find the function $E(t)$ that best fits the measured stress values σ_n . This error function appropriately captures the relationship between adjacent modulus values, but does not specify their offset since the recursive base case is not included. Obtaining the curve fit will therefore be a constrained optimization task where $E(M\Delta t) = \sigma_M$ which assumes measurements have been continued until a steady-state has been reached. A feedforward multilayer perceptron artificial neural network (ANN) with output

$$N(\boldsymbol{\theta}, t) = \sum_{i=1}^h \left[\frac{v_i}{1 + e^{-(w_i t + u_i)}} + x_i \right] \quad (19)$$

is trained where h is the number of hidden nodes, w_i and u_i are the input weights and biases respectively, and v_i and x_i are the output weights and biases respectively. Note that the ANN output N is a function of both time t and the parameter vector $\boldsymbol{\theta}$ containing all the weights and biases. The parameter vector is optimized to minimize the error function S using the Levenberg-

Marquardt gradient descent method (Jang, Sun, and Mitzutani, 1997). In order to handle the optimization constraint, the trial relaxation modulus is defined as

$$E(\boldsymbol{\theta}, t) = (t - M\Delta t)N + \sigma_M \quad (20)$$

Note that E automatically satisfies the constraint regardless of ANN output, simplifying the optimization required of the ANN (McFall, Mahan, 2009). The parameter vector $\boldsymbol{\theta}_0$ is initialized to small random values and updated according to Levenberg-Marquardt by

$$\boldsymbol{\theta}_{i+1} = \boldsymbol{\theta}_i - \eta \left(2\mathbf{J}^T \mathbf{J} + \lambda \mathbf{I} \right)^{-1} \frac{\partial S}{\partial \boldsymbol{\theta}_i} \quad (21)$$

where the rows of Jacobian matrix \mathbf{J} consist of $\partial G_n / \partial \boldsymbol{\theta}_i$ which can be determined analytically from Eqns. (18), (19), and (20). Also note that the error gradient is similarly defined as

$$\frac{\partial S}{\partial \boldsymbol{\theta}_i} = 2 \sum_{n=n_0+1}^M \left(G_n \frac{\partial G_n}{\partial \boldsymbol{\theta}_i} \right) \quad (22)$$

ANN design parameters are h , η , and λ for which values of 10, 0.005, and 0.01 respectively are used for all calculations. The number of hidden neurons h indicates the complexity of the functional relationship between the input and output of the ANN. In general, larger values of h risk overfitting the data. However, the high sampling rate of collected data used to train the ANN precludes any overfitting; the primary drawback of choosing a large h is increased computational time for training. The learning rate η is a measure of the size of changes in the parameter vector $\boldsymbol{\theta}$ and must be chosen small enough to allow convergence on a solution; again the drawback of choosing η too small is increased computation time. The final design parameter, λ distinguishes the learning algorithm as Levenberg-Marquardt where $\lambda = 0$ reduces to Gauss-Newton training and $\lambda = \infty$ represents pure gradient descent. Gradient descent is often trapped in local minima and Gauss-Newton assumes the current parameter vector $\boldsymbol{\theta}$ is already “close” to its optimal value. Levenberg-Marquardt speeds up training as a balance between the two extremes. Being caught in local minima is somewhat sensitive to selection of λ , however ANN solutions are easily checked for validity. The exact values used for h , η , and λ are not crucial since overfitting is essentially impossible due to the small Δt and the fitness of the resulting relaxation modulus can be easily verified by applying the convolution integral to it and checking agreement with the measured stress values.

The measured stress values when linearly ramping strain to a constant value are curve fit using the ANN to obtain the time dependent relaxation modulus as appears in Figure 6.3. Also in Figure 6.3, the relaxation modulus for the standard linear solid model with the same initial and steady-state state moduli as well as a time constant matching the curve fit results. Note that relaxation in the GAB material does decline rapidly, but not quite at the exponential pace of the standard linear solid model. In order to confirm the validity of the curve fit, the convolution integral of the relaxation modulus is compared against the measured stress values in Figure 6.4. Both curves are essentially coincident during the applied constant strain, indicating a successful fit. The convolution integral at times during the strain ramping indicate what the stress would be in the material if it did not exhibit the nonlinear behavior associated with collapsing the void in the aggregate.

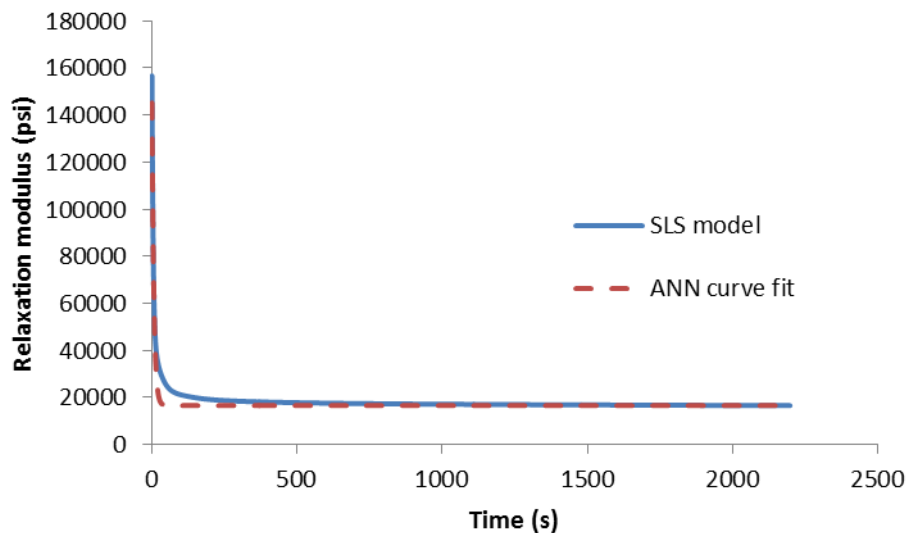


Figure 6.3 Relaxation Modulus Resulting from the ANN Curve Fit of Measured Stress Data Compared With the Standard Linear Solid Model With the Same Time Constant.

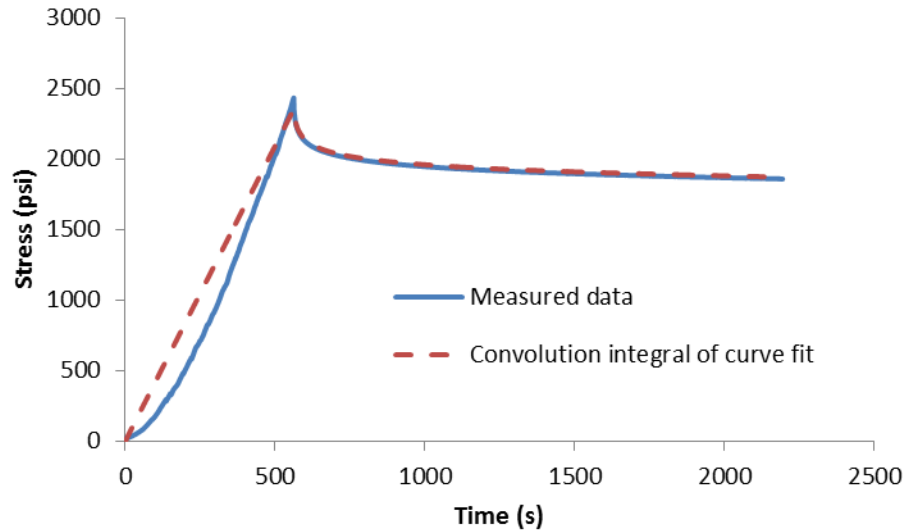


Figure 6.4 Convolution Integral of the Curve Fit Relaxation Modulus Compared with the Measured Stress Values.

6.3 Comparison with Resilient Modulus Test Results

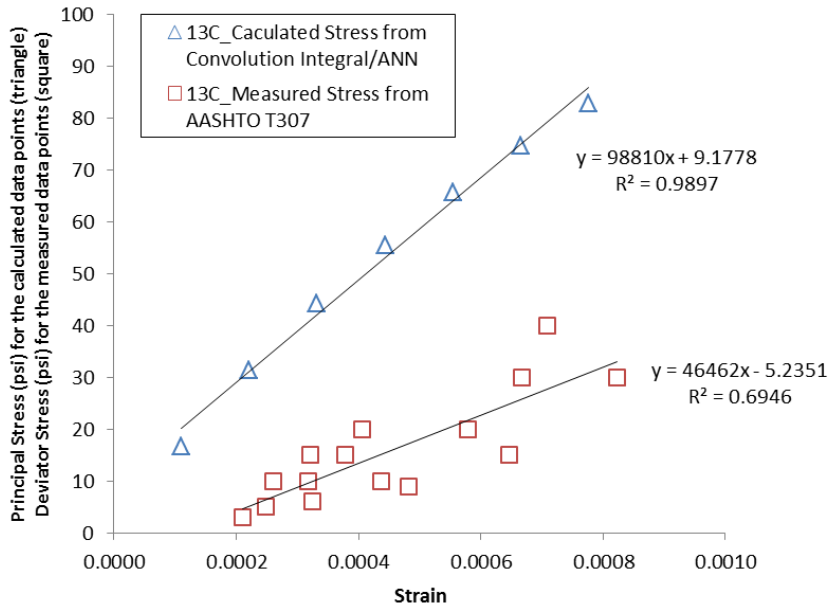
The calculated stresses from the convolution integral of the relaxation modulus resulting from the ANN model were compared with ones obtained from resilient modulus test procedure. The resilient tests were performed using a 150-mm diameter by 300-mm high cylindrical GAB specimens. The AASHTO T307-99 specifies fifteen (15) static stress states to determine stress sensitivity. At each static stress state, deviatoric stresses are applied to the specimen and resilient strains are measured. A loading cycle of dynamic stress consists of 0.1 seconds loading and 0.9 seconds unloading period. One-thousand (1000) load repetitions were applied for conditioning of the specimens, and the deviator and confining stress were held at 103.4 kPa to eliminate the effects of initial permanent deformation. After the conditioning, one-hundred (100) load repetitions were applied to the specimen for each load sequence as shown in Table 3.

The stress-strain relation was determined from the resilient modulus test and compared with ones calculated from the convolution integral of the relaxation modulus as shown in Figures 6.5a and 6.5b.

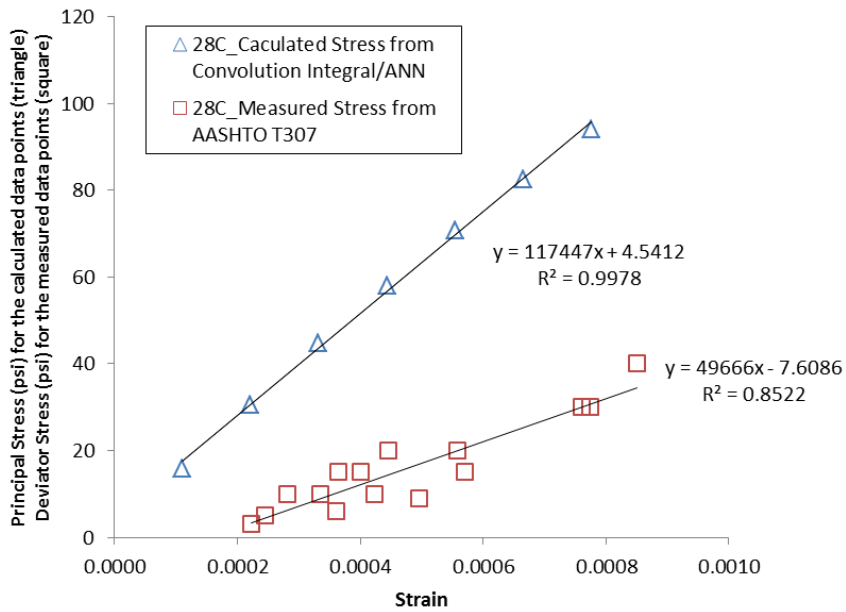
Table 6.2 AASHTO T307-99 Stress States

Test Sequence	σ_1 (kPa)	σ_3 (kPa)	σ_1 (psi)	σ_3 (psi)	Number of Cycles
1	41.4	20.7	6	3	500-1000
2	62.1	20.7	9	3	100
3	82.8	20.7	12	3	100
4	69.0	34.5	10	5	100
5	103.5	34.5	15	5	100
6	137.9	34.5	20	5	100
7	137.9	68.9	20	10	100
8	206.8	68.9	30	10	100
9	275.8	68.9	40	10	100
10	172.4	103.4	25	15	100
11	206.8	103.4	30	15	100
12	310.3	103.4	45	15	100
13	241.3	137.9	35	20	100
14	275.8	137.9	40	20	100
15	413.7	137.9	60	20	100

For comparison purposes, simple linear regression was performed for both calculated and measured stress-strain data pairs for the range of strains tested as shown in Figs.6a and 6b. The slope of the linear regression lines indicates the modulus of the material for the range of stresses tested. Per the definition of the resilient modulus, deviator stress is applied to the specimen, which is the difference between the major principle stress (σ_1) and the confining stress (σ_3). In AASHTO T 307, σ_3 is approximately 25 to 60% of σ_1 during the test procedure. In contrast, one can intuitively observe that σ_3 under CBR and relaxation modulus test is higher than σ_3 under resilient modulus test, which is high degree of anisotropy condition. This condition explains why higher vertical load should be needed in relaxation modulus test to make the same amount of deformation in resilient modulus test procedure. Therefore, this phenomenon can lead to the conclusion that the slopes for the calculated values from the convolution integral of the relaxation modulus test are consistently higher than those of the measured values from the resilient modulus test.



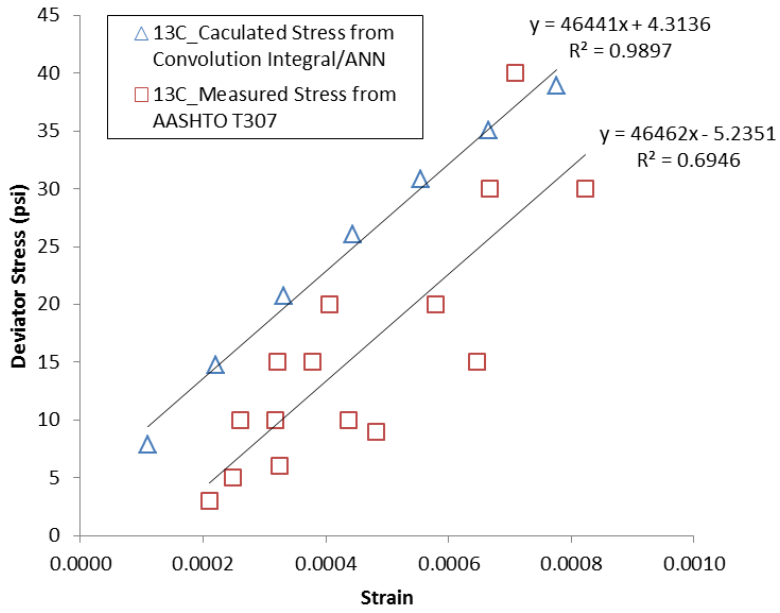
(a) 013C Material



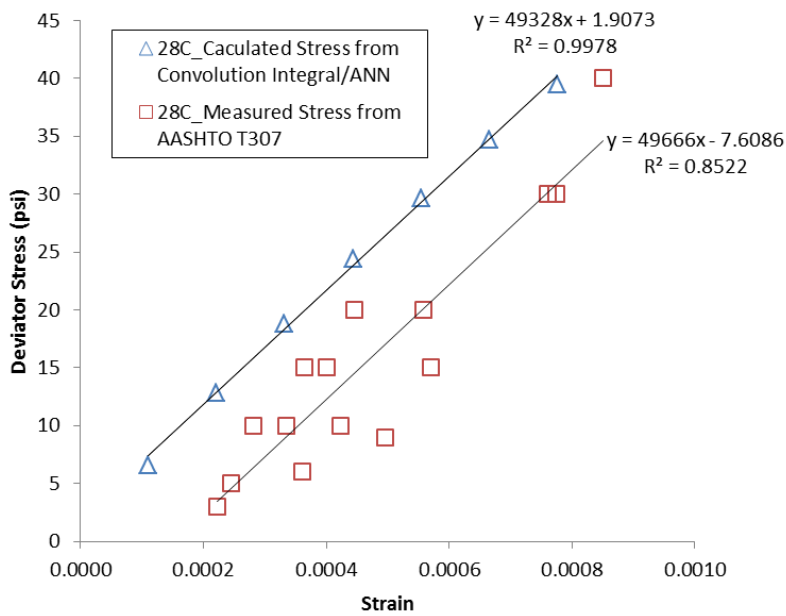
(b) 028C Material

Figure 6.5 Comparison of Measured and Calculated Stresses along with Strain

For direct comparison, deviator stress was calculated by assuming σ_3 as approximately 45% of σ_1 and re-plotted in Figures 6.6a and 6.6b. As shown in Figs. 7a and 7b, the data trends are quite comparable with nearly same slopes, indicating same modulus and the consistency of the stress-strain relationship from the resilient modulus test and the convolution integral based on linear viscoelastic theory. However, the two lines were offset by approximately 10 psi, which is likely due to the difference between the two test protocols and settings. For example, the resilient modulus test requires 15 stress states to be controlled, including both repeated vertical stress and variable confining stresses. On the other hand, the relaxation modulus test only records the vertical principal stress, which results in different stress states than the resilient modulus test. Given the consistency of the test results, the developed methodology could be used to verify the resilient modulus test result in terms of stiffness through relaxation modulus test by considering σ_3 as approximately 45% of σ_1 .



(c) 013C Material



(d) 028C Material

Figure 6.6 Comparison of Measured and Calculated Deviator Stresses along with Strain

7.0 CONCLUSIONS AND RECOMMENDATIONS

In the study, the effects of No. 810 screening contents in GAB on pavement performance and GAB strength were investigated. One Group I (013C) source and three Group II sources (028C, 048C, and 158C) were selected and specimens were fabricated and tested for CBR.

- Proctor and CBR tests were conducted and pavement performance with/without screening materials was simulated by MEPDG using measured CBR.
- Morphological analysis indicated that Group I (013C) source has significantly lower angularity and surface texture compared to Group II sources (028C, 048C, 158C).
- Replacing 25% of Group I GAB (013C) with No. 810 screening materials increased the density of the assembly and resulted in the reduced percentage of alligator cracking. However, the reduced percentage of alligator cracking still exceeded the failure criterion.
- Replacing 25% of Group II GAB (028C, 048C, 158C) with No. 810 screening materials decreased the density of the assemblies and increased alligator cracking. Although alligator cracking increased, it was still below the failure threshold. Nevertheless, the gradation of mixed aggregate assemblies with 25% of screening materials didn't meet the GDOT's GAB gradation requirement.
- To meet the GDOT's GAB gradation requirement for Group II sources, a lower amount of screening materials up to 10% may be considered. However, caution should be used and further investigations, such as those focusing on the permeability, plasticity index, resilient modulus, and life cycle cost analysis, may be needed prior to the adoption of any screening materials in GAB.
- A new methodology was developed to evaluate constitutive relations of GAB materials using linear viscoelastic principles. It has demonstrated that linear viscoelastic principles could be applied to establish the stress-strain relation for aggregate bases using relaxation modulus test that can be easily conducted using CBR apparatus. Thus, the methodology has a potential to estimate aggregate resilient modulus based on constitutive relations. This enables pavement engineers to validate the resilient modulus of aggregate bases obtained from resilient modulus tests using available CBR equipment. Alternatively, the methodology, once calibrated, could be used to estimate the design life of pavement for rehabilitation or forensic investigation.

8.0 REFERENCES

1. Hicks, R. G. and Monismith, C. L. Factors Influencing the Resilient Properties of Granular Materials. In Transportation Research Record 345, Transportation Research Board, National Research Council, Washington, DC, 1971, pp. 15-31.
2. Dawson, A. R. Unbound Aggregates in Road. Balkema, Rotterdam, London, 2000.
3. Barksdale, R. D., and Itani, S. Y. Influence of Aggregate Shape on Base Behaviour. In Transportation Research Record 1227, TRB, National Research Council, Washington, DC, 1989, pp. 173-182.
4. Haynes, J. G., and Yoder, E. J. Effects of Repeated Loading on Gravel and Crushed Stone Base Course Materials Used in the AASHO Road Test. In Highway Research Record 39, National Research Council, HRB, 1963. PP. 82-86.
5. Raad, L., Minassian, G., and Gartin, S. Characterization of Saturated Granular Bases under Repeated Loads. In Transportation Research Record 1369, TRB, National Research Council, Washington, DC, 1992, pp. 73-82.
6. Kolisoja, P. Resilient Deformation Characteristics of Granular Materials. PhD Dissertation, Tampere University of Technology, Tampere, Finland, 1997.
7. Thom, N. H., and Brown, S. F. Effect of Moisture on the Structural Performance of a Crushed-Limestone Road Base. In Transportation Research Record 1121, TRB, National Research Council, Washington, DC, 1987, pp. 50-56.
8. Hicks, R. G. and Monismith, C. L. Factors Influencing the Resilient Properties of Granular Materials. In Transportation Research Record 345, Transportation Research Board, National Research Council, Washington, DC, 1971, pp. 15-31.
9. Sung-Hee Kim. Determination of Aggregate Physical Properties and Its Effect on Cross-Anisotropic Behavior of Unbound Aggregate Materials. Ph.D., Dissertation, Texas A&M University, College Station, TX, 2004.
10. Lekarp, F., Richardson, I. R., and Dawson, A. Influence on Permanent Deformation Behavior of Unbound Granular Materials. In Transportation Research Record 1547, TRB, National Research Council, Washington, DC, 1996, pp. 68-75.
11. Al-Rousan, T., Masad, E., Tutumluer, E., and Pan, T. (2007). "Evaluation of Image Analysis Techniques for Quantifying Aggregate Shape Characteristics," Journal of Construction and Building Materials, Vol. 21, pp. 978-990, 2007.

12. American Association of State and Highway Officials (AASHTO). AASHTO Guide for Design of Pavement Structures. American Association of State and Highway Officials, Washington, DC, 1993.
13. Al-Rousan, T., Masad, E., Tutumluer, E., and Pan, T. (2007). "Evaluation of Image Analysis Techniques for Quantifying Aggregate Shape Characteristics," *Journal of Construction and Building Materials*, Vol. 21, pp. 978-990, 2007.
14. Findley, W., Lai, J., Onaran, K., *Creep and Relaxation of Nonlinear Viscoelastic Materials*, Amsterdam, North-Holland Publishing, 1976.
15. Funahashi, K. On the Approximate Realization of Continuous Mappings by Neural Networks. *Neural Networks*, Vol. 2, No. 3, 1989, pp. 183–192.
16. Hornik, K., M. Stinchcombe, and H. White. Multilayer Feedforward Networks Are Universal Approximators. *Neural Networks*, Vol. 2, No. 5, 1989, pp. 359–366.
17. Jang, J., Sun, C., Mizutani, E., *Neuro-Fuzzy and Soft Computing*, Englewood Cliffs, NJ, Prentice-Hall, 1997.
18. Kim, S., Tutumluer, E., Little D., Effect of Gradation on Nonlinear Stress-Dependent Behavior of a Sandy Flexible Pavement Subgrade, *Journal of Transportation Engineering*, American Society of Civil Engineering, Vol. 133, No. 10, Oct 1, 2007.
19. Kim, S. (2013). Measurements of Dynamic and Resilient Moduli for Roadway Test Sections (Final Report). GDOT Research Project No. 12-07
20. McFall, K., Mahan, J. R., Artificial Neural Network Method for Solution of Boundary Value Problems with Exact Satisfaction of Arbitrary Boundary Conditions, *IEEE Transactions on Neural Networks*, Vol. 20, No. 8, August 2009
21. MacKay D. J. C., A Practical Bayesian Framework for Backpropagation Networks, *Neural Computation* 4, 1992, pp. 448-472
22. NeuroShell 2, Software by Ward Systems Group, Inc.
23. Xiao, Y., Tutumluer, E. and J. Siekmeier. Resilient Modulus Behavior Estimated from Aggregate Source Properties, *Proceedings of the ASCE Geo-Frontiers 2011 Conference*, Dallas, Texas, March 13-16, 2011

APPENDIX A

Image Analysis Results

Image Analysis Result (013C)

Retained on 19mm Sieve

Retained on 12.5mm Sieve

Retained on 4.75mm Sieve

Retained on 19mm Sieve								Retained on 12.5mm Sieve								Retained on 4.75mm Sieve										
Particle	Angularity	Sieve	S Max	FE Ratio	S Min	Volume	Area	Surf Texture	Particle	Angularity	Sieve	S Max	FE Ratio	S Min	Volume	Area	Surf Texture	Particle	Angularity	Sieve	S Max	FE Ratio	S Min	Volume	Area	Surf Texture
1	518.37	1.24	1.83	2.60	0.71	0.69	8.87	2.66	1	419.34	0.53	0.76	2.41	0.32	0.06	1.46	1.63	1	524.02	0.59	0.98	3.43	0.28	0.05	1.45	4.36
2	384.73	1.01	1.18	1.52	0.78	0.30	3.66	1.52	2	377.40	0.81	1.42	3.53	0.40	0.22	5.17	2.18	2	440.10	0.59	0.93	2.92	0.32	0.07	1.95	3.45
3	403.00	0.85	1.12	2.85	0.39	0.15	2.55	1.48	3	415.23	0.71	0.92	2.17	0.43	0.11	1.92	1.26	3	681.48	0.62	0.82	2.16	0.38	0.10	1.89	3.54
4	416.01	0.79	1.10	1.62	0.68	0.21	3.30	1.45	4	485.81	0.63	0.88	1.97	0.45	0.09	1.66	1.84	4	422.68	0.53	1.31	3.47	0.38	0.09	2.35	3.26
5	529.20	0.96	1.27	2.09	0.61	0.25	3.88	2.21	5	419.96	0.77	1.29	2.67	0.48	0.19	5.44	2.22	5	610.13	0.66	0.85	1.62	0.53	0.08	1.74	2.95
6	395.66	0.89	1.28	4.34	0.29	0.14	4.24	1.53	6	319.38	0.79	1.17	2.97	0.39	0.16	2.49	1.67	6	306.54	0.56	0.84	2.25	0.37	0.08	2.18	2.18
7	439.49	0.88	1.36	2.05	0.66	0.24	3.34	1.95	7	413.44	0.54	0.74	1.88	0.39	0.05	1.20	1.64	7	365.73	0.63	0.87	2.58	0.34	0.07	1.65	1.98
8	410.35	0.82	1.37	2.47	0.55	0.24	3.60	1.44	8	431.92	0.73	1.06	3.86	0.27	0.07	1.69	2.90	8	355.37	0.73	0.96	2.22	0.43	0.11	1.99	1.46
9	332.25	0.88	1.30	3.03	0.43	0.21	3.22	1.40	9	422.91	0.73	1.08	3.00	0.36	0.11	2.36	2.65	9	570.56	0.67	0.96	2.78	0.35	0.08	2.28	4.41
10	319.46	0.94	1.33	4.68	0.28	0.15	4.29	1.73	10	340.47	0.73	1.03	2.62	0.39	0.12	2.05	1.66	10	502.29	0.62	1.01	2.21	0.46	0.12	2.36	2.13
11	598.41	1.10	1.33	2.02	0.66	0.32	4.30	1.97	11	279.25	0.52	0.76	2.69	0.28	0.05	1.12	1.36	11	438.33	0.58	0.80	2.29	0.35	0.07	1.51	3.10
12	398.50	1.12	1.62	2.39	0.68	0.48	4.87	1.55	12	333.96	0.88	1.30	2.99	0.43	0.23	3.43	1.27	12	487.03	0.73	0.90	2.31	0.39	0.10	1.56	2.48
13	350.05	0.88	1.41	2.20	0.64	0.31	3.75	1.51	13	385.22	0.98	1.28	1.97	0.65	0.24	4.87	2.02	13	561.83	0.49	0.97	2.63	0.37	0.06	1.91	3.74
14	448.31	0.94	1.69	2.73	0.62	0.41	4.76	1.97	14	445.89	0.96	1.25	2.00	0.62	0.30	3.52	1.32	14	341.85	0.55	0.82	2.13	0.38	0.06	1.27	1.81
15	496.86	1.09	1.68	4.21	0.40	0.35	5.73	2.15	15	434.58	0.74	1.33	3.53	0.38	0.15	2.58	1.89	15	525.49	0.55	1.25	3.91	0.32	0.06	1.70	4.06
16	364.16	1.12	1.44	2.17	0.66	0.39	4.46	1.51	16	460.85	0.81	1.17	4.94	0.24	0.08	1.45	2.66	16	562.83	0.55	0.80	1.86	0.43	0.07	1.80	2.89
17	387.06	1.12	1.83	3.31	0.55	0.50	5.86	1.71	17	498.74	0.76	1.40	4.07	0.34	0.15	2.53	2.41	17	446.23	0.62	0.77	2.02	0.38	0.07	1.54	2.22
18	464.97	0.95	1.23	2.26	0.54	0.32	3.60	1.54	18	369.15	0.65	1.04	2.53	0.41	0.09	1.76	2.14	18	499.59	0.46	0.78	2.47	0.31	0.05	1.33	3.49
19									19	334.69	0.85	1.05	3.51	0.30	0.09	2.14	1.63	19	506.24	0.63	1.00	3.19	0.31	0.08	2.21	2.74
20									20	432.15	0.68	0.97	1.88	0.51	0.13	2.15	1.84	20	413.18	0.60	0.76	2.03	0.37	0.08	1.57	2.07
21									21	395.34	0.56	0.86	2.14	0.40	0.06	1.22	1.91	21	396.58	0.57	0.75	2.26	0.33	0.07	1.32	2.92
22									22	508.70	0.58	0.84	2.40	0.35	0.07	1.57	1.92	22	596.69	0.73	1.09	3.81	0.29	0.07	1.69	3.11
23									23	386.44	0.53	0.78	1.91	0.41	0.07	1.51	1.86	23	401.10	0.61	0.88	2.29	0.38	0.05	1.56	2.08
24									24	401.59	0.65	0.88	1.97	0.45	0.09	1.94	1.26	24	420.28	0.61	0.94	3.09	0.31	0.08	1.89	2.41
25									25	493.20	0.51	0.90	2.51	0.36	0.06	1.66	2.54	25	538.45	0.51	0.72	2.46	0.29	0.04	1.43	4.20
26									26	502.70	0.83	1.19	6.01	0.20	0.08	2.37	3.18	26	398.44	0.67	0.93	3.35	0.28	0.08	1.93	4.05
27									27	523.95	0.54	1.02	3.17	0.32	0.08	1.64	2.60	27	494.90	0.61	0.92	2.73	0.34	0.06	1.53	3.92
28									28	500.87	0.58	0.91	4.71	0.19	0.04	1.17	2.40	28	541.66	0.47	0.61	1.52	0.40	0.05	1.20	3.01
29									29	469.38	0.60	1.01	3.28	0.31	0.07	2.27	3.09	29	478.50	0.44	1.06	3.63	0.29	0.04	1.26	4.31
30									30	354.88	0.72	0.96	3.55	0.27	0.09	1.58	1.39	30	429.55	0.67	0.98	2.84	0.34	0.07	1.29	2.40
31									31	335.47	0.58	0.97	1.93	0.50	0.12	2.35	1.64	31	573.92	0.67	0.93	3.70	0.25	0.06	1.60	3.49
32									32	436.33	0.64	0.86	3.18	0.27	0.06	1.40	1.88	32	656.32	0.58	0.83	2.62	0.32	0.06	1.36	4.51
33									33	516.92	0.63	0.87	3.04	0.29	0.05	1.99	3.52	33	595.70	0.53	0.86	3.05	0.28	0.05	1.86	5.38
34									34	495.37	0.58	0.96	2.06	0.47	0.11	1.94	2.21	34	658.85	0.43	0.85	2.80	0.31	0.04	1.21	5.31
35									35	362.26	0.70	0.93	3.87	0.24	0.06	1.76	2.60	35	431.85	0.54	0.71	1.63	0.43	0.06	1.29	2.04
																		36	495.29	0.59	1.02	3.85	0.27	0.04	1.38	3.39
																		37	538.97	0.51	0.61	1.39	0.44	0.05	1.11	2.11
																		38	438.29	0.49	0.75	3.08	0.24	0.03	1.03	3.16



Max	598.41	1.24	1.83	4.68	0.78	0.69	8.87	2.66	Max	523.95	0.98	1.42	6.01	0.65	0.30	5.44	3.52	Max	681.48	0.73	1.31	3.91	0.53	0.12	2.36	5.38
Min	319.46	0.79	1.10	1.52	0.28	0.14	2.55	1.40	Min	279.25	0.51	0.74	1.88	0.19	0.04	1.12	1.26	Min	306.54	0.43	0.61	1.39	0.24	0.03	1.03	1.46
Avg	425.38	0.98	1.41	2.70	0.56	0.31	4.35	1.74	Avg	420.11	0.69	1.02	2.94	0.37	0.11	2.21	2.06	Avg	490.71	0.58	0.89	2.65	0.35	0.07	1.64	3.16
COV	16.77	12.65	15.69	32.81	25.32	43.76	31.56	19.27	COV	15.16	18.10	18.27	32.71	27.90	56.44	47.85	27.97	COV	18.42	13.13	16.27	25.43	17.75	29.59	21.45	30.58

Image Analysis Result (028C)

Retained on 19-mm Sieve										Retained on 12.5-mm Sieve										Retained on 4.75-mm Sieve									
Particle	Angularity	Sieve	S Max	FE Ratio	S Min	Volum	Area	Surf Tex	Particle	Angularity	Sieve	S Max	FE Ratio	S Min	Volum	Area	Surf Tex	Particle	Angularity	Sieve	S Max	FE Ratio	S Min	Volum	Area	Surf Te			
1	587.11	0.96	1.21	2.17	0.56	0.21	5.29	2.14	1	305.22	0.74	1.23	2.76	0.45	0.16	2.54	1.43	1	511.87	0.83	1.13	4.24	0.27	0.10	2.50	2.87			
2	572.40	1.07	1.88	3.36	0.56	0.50	6.98	3.09	2	445.39	0.78	1.67	4.37	0.38	0.26	4.33	2.01	2	444.14	0.64	1.09	2.92	0.37	0.11	2.53	2.24			
3	538.11	1.12	1.37	2.13	0.64	0.38	7.15	3.18	3	477.26	0.68	1.56	2.59	0.60	0.23	8.19	1.95	3	426.25	0.61	0.83	1.99	0.42	0.07	1.55	1.76			
4	398.64	0.88	1.76	2.96	0.60	0.39	4.94	1.71	4	443.57	0.69	1.05	2.02	0.52	0.15	3.07	2.67	4	451.07	0.51	1.09	3.11	0.35	0.06	2.73	3.27			
5	540.13	0.83	1.53	2.88	0.53	0.27	4.55	2.54	5	380.94	0.80	1.09	2.52	0.43	0.13	2.41	2.09	5	494.28	0.50	0.92	2.62	0.35	0.06	2.46	3.58			
6	536.34	1.12	1.76	4.10	0.43	0.38	5.71	2.64	6	471.95	0.70	0.92	1.42	0.64	0.14	2.37	1.58	6	476.59	0.66	0.92	2.37	0.39	0.08	1.72	2.02			
7	376.63	1.27	2.04	3.49	0.58	0.62	7.57	1.92	7	448.18	0.52	1.13	2.46	0.46	0.08	1.49	2.93	7	557.71	0.67	1.21	2.98	0.40	0.12	2.37	3.03			
8	446.60	0.88	1.87	4.11	0.46	0.33	6.22	2.84	8	445.55	0.59	0.80	1.94	0.42	0.07	2.08	2.31	8	580.26	0.72	1.16	2.28	0.51	0.13	3.12	4.42			
9	506.61	0.88	1.37	2.46	0.56	0.26	4.94	2.88	9	490.70	0.56	0.91	2.26	0.40	0.08	1.50	2.21	9	552.47	0.67	0.86	2.09	0.41	0.07	1.61	2.21			
10	299.19	0.90	1.27	2.32	0.55	0.30	3.77	0.97	10	470.92	0.62	1.02	3.29	0.31	0.06	2.23	3.12	10	619.68	0.55	0.81	2.02	0.40	0.05	1.65	5.25			
11	506.49	0.78	1.00	1.86	0.54	0.12	3.46	2.18	11	393.17	0.88	1.33	4.91	0.27	0.14	3.16	2.70	11	491.32	0.54	0.92	2.88	0.32	0.05	1.33	2.98			
12	407.42	1.06	1.40	2.54	0.55	0.36	5.14	2.21	12	477.18	0.80	1.17	3.21	0.36	0.10	2.41	3.00	12	504.09	0.56	0.75	2.10	0.36	0.06	1.77	2.85			
13	383.75	1.00	1.88	3.94	0.48	0.47	5.60	1.92	13	401.06	0.62	1.10	3.44	0.32	0.08	1.76	2.16	13	610.18	0.59	0.64	2.40	0.27	0.04	1.27	3.72			
14	427.57	1.67	1.97	2.40	0.82	1.35	10.89	1.63	14	495.17	0.67	0.95	2.22	0.43	0.13	2.27	1.79	14	652.01	0.47	0.73	1.96	0.37	0.05	1.15	4.29			
15	497.33	1.08	1.83	2.39	0.77	0.64	7.06	1.93	15	537.22	0.80	1.33	3.32	0.40	0.17	2.87	2.16	15	496.95	0.52	0.88	4.06	0.22	0.04	1.46	5.00			
16	416.57	1.07	1.45	2.32	0.62	0.41	4.49	1.44	16	419.46	0.65	1.14	2.44	0.47	0.13	2.30	2.32	16	528.70	0.56	0.85	2.67	0.32	0.05	1.21	2.75			
17	350.83	0.99	1.37	3.97	0.35	0.20	4.10	1.77	17	474.86	0.65	0.80	1.36	0.59	0.10	1.67	1.68	17	525.57	0.46	0.60	1.85	0.32	0.04	1.14	3.81			
18									18	457.56	0.67	1.18	4.63	0.25	0.09	3.27	3.17												
19									19	413.35	0.62	1.36	3.23	0.42	0.14	2.91	2.70												
20									20	502.93	0.69	0.83	2.22	0.37	0.10	1.85	1.74												
21									21	435.77	0.64	0.82	2.50	0.33	0.07	1.50	2.17												
22									22	422.00	0.58	1.00	2.24	0.45	0.12	1.70	1.28												
23									23	424.35	0.65	0.98	2.33	0.42	0.14	2.16	1.56												
24									24	558.60	0.77	1.13	2.14	0.53	0.20	2.92	1.85												
25									25	512.25	0.60	1.16	3.17	0.36	0.13	2.73	2.70												
26									26	592.68	0.76	0.90	1.96	0.46	0.11	2.35	2.42												
27									27	391.75	0.75	1.01	1.99	0.51	0.17	2.47	1.48												
28									28	379.14	0.68	0.90	1.39	0.65	0.16	2.31	1.26												
29									29	559.64	0.53	1.10	3.74	0.29	0.06	1.54	3.38												
30									30	506.03	0.52	0.79	1.97	0.40	0.07	2.45	1.98												
31									31	505.34	0.53	0.70	1.95	0.36	0.07	1.38	2.14												
32									32	552.86	0.58	0.85	2.16	0.39	0.10	2.03	1.73												
33									33	333.17	0.55	0.97	2.17	0.45	0.11	2.03	2.14												
34									34	339.86	0.61	1.05	4.57	0.23	0.07	1.86	3.15												
35									35	449.26	0.81	1.36	5.75	0.24	0.13	2.91	2.87												
36									36	405.35	0.70	0.84	1.93	0.44	0.10	2.97	1.96												
37									37	499.58	0.59	1.06	2.49	0.43	0.10	3.43	2.53												
38									38	569.82	0.78	1.29	4.91	0.26	0.10	2.80	2.54												
39									39	473.12	0.71	0.95	5.16	0.18	0.05	1.66	3.55												
40									40	461.01	0.86	1.46	4.30	0.34	0.22	3.92	2.16												
41									41	532.77	0.69	1.44	4.02	0.36	0.15	2.71	3.03												
42									42	528.37	0.49	0.73	1.60	0.46	0.06	1.33	2.02												
43									43	414.58	0.56	1.04	2.90	0.36	0.08	2.00	1.87												
44									44	392.65	0.50	0.72	2.35	0.31	0.05	1.22	1.76												
45									45	584.59	0.61	0.92	1.99	0.46	0.09	2.01	3.58												
46									46	427.47	0.69	1.19	3.72	0.32	0.10	1.99	2.61												
47									47	549.86	0.60	0.88	2.17	0.40	0.08	1.59	2.30												
48									48	480.74	0.61	0.76	2.35	0.32	0.05	1.30	3.06												
49									49	442.49	0.61	0.77	3.10	0.25	0.04	1.36	2.80												
50									50	614.64	0.78	1.03	3.62	0.28	0.07	2.42	2.73												
51									51	476.79	0.66	0.85	3.8	0.22	0.05	1.59	2.55												



Max	587.11	1.67	2.04	4.11	0.82	1.35	10.89	3.18	Max	614.64	0.88	1.67	5.75	0.65	0.26	8.19	3.58	Max	652.01	0.83	1.21	4.24	0.51	0.13	3.12	5.25
Min	299.19	0.78	1.00	1.86	0.35	0.12	3.46	0.97	Min	305.22	0.49	0.70	1.36	0.18	0.04	1.22	1.26	Min	426.25	0.46	0.60	1.85	0.22	0.04	1.14	1.76
Avg	458.34	1.03	1.59	2.91	0.56	0.42	5.76	2.18	Avg	466.04	0.66	1.04	2.88	0.39	0.11	2.38	2.33	Avg	524.89	0.59	0.91	2.62	0.36	0.07	1.86	3.30
COV	17.79	19.42	18.78	25.60	19.31	63.42	30.38	27.30	COV	14.50	14.43	21.51	36.81	26.90	43.99	44.84	25.05	COV	11.76	15.96	19.25	25.84	18.47	40.29	32.75	30.00

Image Analysis Result (048C)

19-mm									12.5-mm									4.75-mm								
Particle	Angularity	Sieve	S Max	FE Ratio	S Min	Volum	Area	Surf Tex	Particle	Angularity	Sieve	S Max	FE Ratio	S Min	Volum	Area	Surf Tex	Particle	Angularity	Sieve	S Max	FE Ratio	S Min	Volum	Area	Surf Te
1	421.57	1.10	2.51	4.07	0.62	0.82	9.07	2.09	1	455.96	0.74	1.09	5.20	0.21	0.05	1.91	3.85	1	570.64	0.64	0.75	1.50	0.50	0.09	1.94	2.43
2	667.81	1.20	1.67	4.35	0.38	0.29	4.73	3.42	2	649.96	0.65	0.79	1.74	0.46	0.08	1.80	3.18	2	502.93	0.67	1.22	3.67	0.33	0.09	2.13	3.22
3	355.95	1.18	1.87	5.50	0.34	0.33	5.55	2.81	3	456.79	0.62	0.87	1.63	0.53	0.11	2.19	1.64	3	394.79	0.68	0.96	2.08	0.46	0.10	2.29	1.98
4	267.79	1.42	1.77	2.34	0.76	0.60	6.39	1.56	4	448.65	0.82	1.38	2.33	0.59	0.24	3.43	1.84	4	471.15	0.58	0.70	1.57	0.45	0.09	2.00	2.28
5	444.88	1.07	2.12	4.40	0.48	0.47	7.39	3.42	5	419.93	0.75	1.18	2.56	0.46	0.15	2.39	1.52	5	442.67	0.58	0.94	2.41	0.39	0.08	1.89	2.22
6	404.79	0.93	1.70	3.36	0.51	0.32	4.89	2.26	6	419.86	0.61	0.94	2.96	0.32	0.07	1.42	1.77	6	415.59	0.71	1.06	2.34	0.45	0.12	2.28	2.20
7	540.65	0.89	1.20	2.40	0.50	0.26	3.48	2.16	7	406.24	0.66	1.12	2.12	0.53	0.18	2.85	1.49	7	386.68	0.69	0.98	2.57	0.38	0.08	2.15	3.18
8	297.71	0.87	1.53	3.32	0.46	0.25	3.24	1.18	8	491.85	0.73	1.45	3.35	0.43	0.16	3.37	3.98	8	497.92	0.64	0.91	2.28	0.40	0.08	1.88	2.25
9	333.54	1.20	1.59	2.41	0.66	0.50	5.78	1.30	9	542.13	0.61	1.07	1.87	0.57	0.14	2.67	2.45	9	371.19	0.70	0.85	2.10	0.40	0.09	2.31	2.14
10	384.09	1.19	1.59	1.78	0.90	0.66	6.67	1.53	10	638.70	0.59	1.02	3.16	0.32	0.07	2.22	2.64	10	506.18	0.61	0.81	2.17	0.37	0.08	1.84	3.04
11	468.92	0.78	1.13	2.43	0.46	0.20	3.00	1.87	11	519.69	0.54	1.17	2.80	0.42	0.10	2.20	2.95	11	418.88	0.57	0.80	2.01	0.40	0.07	1.33	2.03
12	434.05	0.86	1.43	2.89	0.50	0.22	4.43	2.75	12	397.22	0.77	1.18	2.87	0.41	0.16	3.14	2.43	12	338.53	0.60	0.76	1.89	0.40	0.09	1.89	1.77
13	452.48	1.28	1.91	2.60	0.73	0.65	6.55	1.62	13	482.03	0.74	1.21	2.39	0.50	0.21	3.11	1.62	13	537.02	0.63	0.87	2.40	0.36	0.09	1.95	3.09
14	493.95	1.29	1.58	3.00	0.53	0.41	5.26	2.07	14	309.36	0.49	0.97	3.04	0.32	0.06	1.48	2.37	14	318.39	0.66	1.17	2.90	0.40	0.10	2.29	2.24
15	457.25	1.01	1.59	2.13	0.75	0.32	4.91	1.69	15	429.58	0.68	1.07	2.99	0.36	0.09	1.70	1.81	15	474.93	0.69	1.08	4.73	0.23	0.07	2.03	4.97
16	387.02	1.03	1.54	2.97	0.52	0.32	4.02	1.69	16	354.09	0.69	1.03	2.64	0.39	0.12	1.82	1.28	16	376.10	0.60	0.91	2.68	0.34	0.08	2.06	3.76
17	349.10	0.87	1.96	2.92	0.67	0.40	5.35	2.11	17	602.40	0.93	1.36	2.87	0.47	0.20	3.24	2.66	17	447.43	0.66	0.87	2.14	0.41	0.07	1.90	2.11
18	497.67	1.48	1.76	4.04	0.43	0.50	7.09	2.78	18	546.14	0.57	1.00	3.63	0.28	0.06	1.67	3.13	18	457.77	0.66	0.89	2.92	0.30	0.08	1.87	2.08
19	443.59	1.05	1.67	2.63	0.63	0.43	5.74	2.40	19	466.22	0.78	1.56	3.46	0.45	0.24	4.60	2.61	19	561.04	0.65	0.78	2.54	0.31	0.08	1.66	3.20
20	310.31	0.94	1.52	2.72	0.56	0.32	4.89	1.98	20	597.01	0.49	0.92	2.06	0.45	0.09	1.64	2.12	20	501.80	0.57	0.73	2.63	0.28	0.05	1.56	3.77
21	393.79	0.87	1.25	3.48	0.36	0.20	3.20	1.46	21	418.13	0.68	0.96	2.44	0.39	0.10	2.31	1.69	21	562.35	0.63	0.87	2.45	0.35	0.08	2.01	2.83
22	584.80	0.84	1.18	3.85	0.31	0.15	3.24	2.80	22	478.50	0.62	1.23	2.94	0.42	0.12	2.28	3.14	22	444.14	0.59	1.03	3.05	0.34	0.07	1.92	2.64
23	365.12	0.98	1.37	2.14	0.64	0.31	6.96	2.21	23	324.80	0.55	0.96	2.50	0.38	0.08	1.80	1.63	23	592.62	0.62	0.82	2.13	0.38	0.08	1.33	2.07
24	423.05	1.05	1.32	2.66	0.50	0.25	3.44	1.51	24	554.15	0.73	0.98	2.75	0.36	0.10	3.13	3.10	24	385.73	0.54	0.66	1.35	0.49	0.07	1.43	1.81
25	565.78	0.86	1.13	4.09	0.28	0.12	2.67	2.04	25	465.21	0.82	1.15	3.05	0.38	0.14	2.98	3.84	25	358.18	0.64	0.91	2.95	0.31	0.06	1.54	1.98
26	287.08	0.89	1.42	5.40	0.26	0.17	3.88	2.55	26	605.86	0.67	0.88	2.60	0.34	0.07	1.45	2.15	26	635.05	0.59	0.73	2.23	0.33	0.07	1.63	3.03
27	501.09	0.86	1.13	1.96	0.58	0.22	2.59	2.00	27	359.64	0.75	1.08	3.70	0.29	0.09	2.10	2.75	27	634.72	0.72	0.96	2.78	0.34	0.06	1.58	4.39
28	346.42	1.14	1.35	1.73	0.78	0.53	5.64	1.42	28	417.87	0.59	0.84	2.43	0.35	0.07	1.51	2.24	28	484.82	0.57	0.76	1.84	0.42	0.05	1.18	2.40
29									29	716.23	0.50	0.90	2.83	0.32	0.06	1.59	2.72	29	349.54	0.54	0.86	2.58	0.33	0.06	1.52	2.50
30									30	557.89	0.55	0.97	2.95	0.33	0.05	1.25	3.14	30	417.10	0.59	0.85	3.02	0.28	0.06	1.23	2.21
31									31	498.80	0.60	0.78	2.58	0.30	0.06	1.30	2.72	31	391.86	0.50	0.87	2.94	0.29	0.05	1.19	1.74
32									32	352.99	0.67	0.96	4.28	0.23	0.06	1.23	2.40	32	605.26	0.64	0.76	2.15	0.35	0.07	1.57	3.38
33									33	438.79	0.68	0.91	2.90	0.31	0.08	1.70	1.73	33	467.85	0.58	0.87	3.90	0.22	0.05	2.34	4.92
34									34	577.97	0.68	1.03	2.88	0.36	0.08	1.79	3.48	34	500.46	0.53	0.79	1.97	0.40	0.08	1.71	2.40
35									35									35	301.52	0.60	0.92	2.92	0.31	0.09	1.98	2.72
36									36									36	475.12	0.63	0.91	3.03	0.30	0.05	1.30	3.22
37									37									37	352.79	0.48	0.96	2.97	0.32	0.06	1.49	2.50
38									38									38	590.68	0.60	0.76	2.59	0.29	0.04	0.98	3.77
39									39									39	392.46	0.58	0.78	2.59	0.30	0.07	1.37	3.42
40									40									40	470.33	0.65	0.83	3.06	0.27	0.06	1.68	4.18
41									41									41	417.63	0.57	0.64	1.48	0.43	0.06	1.54	3.06
42									42									42	588.43	0.76	0.98	3.45	0.28	0.09	2.29	3.37
43									43									43	522.40	0.53	0.80	2.41	0.33	0.03	1.03	3.05
44									44									44	586.37	0.53	1.02	3.96	0.26	0.05	1.46	4.21
45									45									45	507.87	0.43	0.75	3.03	0.25	0.04	1.07	4.35
46									46									46	501.50	0.65	0.83	2.27	0.37	0.07	1.78	2.97



Max	667.81	1.48	2.51	5.50	0.90	0.82	9.07	3.42	Max	716.23	0.93	1.56	5.20	0.59	0.24	4.60	3.98	Max	635.05	0.76	1.22	4.73	0.50	0.12	2.34	4.97
Min	267.79	0.78	1.13	1.73	0.26	0.12	2.59	1.18	Min	309.36	0.49	0.78	1.63	0.21	0.05	1.23	1.28	Min	301.52	0.43	0.64	1.35	0.22	0.03	0.98	1.74
Avg	424.29	1.04	1.56	3.13	0.54	0.37	5.00	2.10	Avg	482.37	0.66	1.06	2.84	0.39	0.11	2.21	2.47	Avg	468.01	0.61	0.87	2.58	0.35	0.07	1.73	2.89
COV	22.02	17.51	20.32	31.74	29.43	46.57	32.00	28.04	COV	20.09	15.16	17.06	24.02	23.14	48.46	35.17	29.43	COV	18.50	10.62	14.08	25.82	18.90	25.05	21.55	28.90

Image Analysis Result (158C)

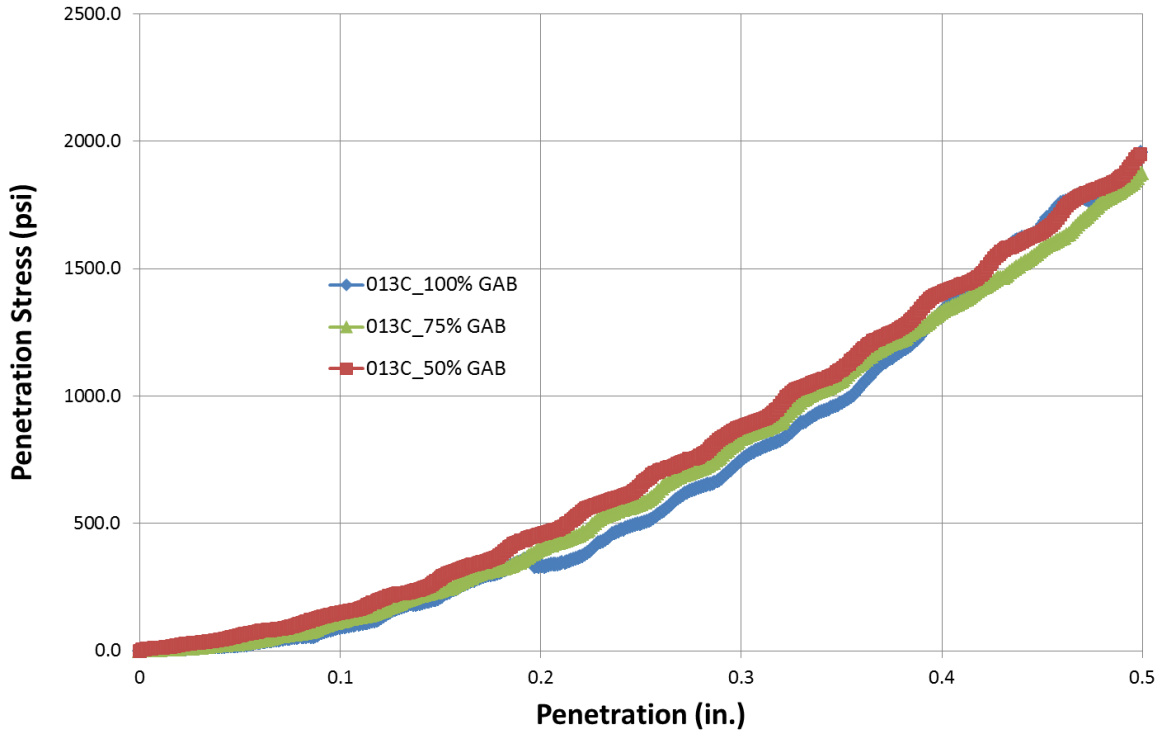
19-mm										12.5-mm										4.75-mm															
Particle	Angularity	Sieve	S	Max	FE Ratio	S	Min	Volume	Area	Surf	Tex	Particle	Angularity	Sieve	S	Max	FE Ratio	S	Min	Volume	Area	Surf	Tex	Particle	Angularity	Sieve	S	Max	FE Ratio	S	Min	Volume	Area	Surf	Tex
1	456.76	1.00	1.45	2.12	0.69	0.46	5.00	1.40	1	406.07	0.65	1.15	2.35	0.49	0.17	2.71	1.60	1	463.11	0.84	1.31	5.27	0.25	0.07	2.03	3.32									
2	322.84	1.11	1.61	2.48	0.65	0.42	4.58	1.50	2	422.14	0.58	0.87	2.40	0.36	0.08	1.75	1.55	2	384.63	0.74	1.02	2.51	0.40	0.11	2.07	2.03									
3	326.56	1.26	2.00	2.84	0.71	0.65	7.08	1.78	3	422.74	0.90	1.28	4.15	0.31	0.13	2.67	2.93	3	388.00	0.60	0.92	2.96	0.31	0.06	1.75	2.50									
4	340.17	1.00	1.48	3.22	0.46	0.30	4.00	1.34	4	407.67	0.72	1.10	2.46	0.45	0.14	2.34	1.66	4	332.01	0.65	1.04	2.66	0.39	0.12	2.16	1.45									
5	529.73	1.11	1.36	2.25	0.60	0.27	4.66	2.17	5	528.81	0.63	1.68	3.49	0.48	0.20	3.53	3.39	5	430.93	0.73	0.96	4.08	0.24	0.07	1.84	3.18									
6	463.18	1.34	1.95	2.39	0.82	0.71	6.88	1.29	6	532.04	0.66	1.03	2.77	0.37	0.11	2.05	2.46	6	570.42	0.69	0.98	2.62	0.37	0.09	2.16	2.65									
7	424.14	0.90	2.10	4.34	0.49	0.37	5.76	3.08	7	454.40	0.77	1.25	3.42	0.36	0.14	2.70	1.94	7	422.76	0.66	0.84	1.81	0.47	0.10	1.92	1.49									
8	450.01	0.86	1.44	2.68	0.54	0.31	4.07	1.63	8	439.39	0.87	1.40	3.44	0.41	0.18	3.98	2.38	8	310.15	0.81	1.15	3.87	0.30	0.09	2.12	2.24									
9	399.46	1.14	1.83	4.29	0.43	0.40	5.29	1.90	9	378.91	0.58	1.41	3.34	0.42	0.15	3.01	2.14	9	457.48	0.62	0.94	1.98	0.47	0.10	2.13	1.91									
10	410.95	1.56	2.22	2.64	0.84	1.33	10.88	1.15	10	320.37	0.74	1.17	3.30	0.35	0.12	2.30	1.81	10	545.37	0.67	0.83	1.81	0.46	0.09	2.02	2.47									
11	407.68	0.99	1.19	1.64	0.72	0.33	4.40	1.44	11	423.30	0.78	1.08	1.89	0.57	0.19	2.73	1.70	11	435.50	0.59	0.73	1.56	0.47	0.08	1.64	1.89									
12	371.59	0.95	1.18	1.58	0.75	0.29	3.63	1.52	12	404.27	0.57	1.04	2.43	0.43	0.10	1.75	1.83	12	546.70	0.66	1.33	2.83	0.47	0.14	2.88	2.91									
13	335.59	1.00	1.73	2.79	0.62	0.47	5.91	1.57	13	487.56	0.70	0.84	3.20	0.26	0.06	1.34	2.07	13	690.39	0.78	1.22	2.31	0.53	0.13	2.92	3.69									
14	436.03	1.19	1.58	3.39	0.47	0.31	4.23	1.96	14	444.56	0.78	1.09	2.39	0.46	0.17	2.79	1.57	14	429.83	0.75	1.03	2.89	0.36	0.09	2.26	2.10									
15	373.31	0.73	1.32	3.82	0.35	0.18	3.05	1.95	15	376.16	0.81	0.97	2.39	0.40	0.13	2.48	1.41	15	427.14	0.71	1.01	1.80	0.56	0.10	1.90	1.78									
16	534.37	0.96	1.81	3.06	0.59	0.41	5.96	2.06	16	477.21	0.73	0.96	2.16	0.45	0.14	2.40	1.56	16	372.28	0.52	0.98	3.38	0.29	0.05	1.24	2.67									
17	364.24	0.95	1.33	3.44	0.39	0.21	3.47	1.81	17	341.44	0.91	1.32	3.94	0.34	0.14	2.08	2.27	17	456.99	0.64	0.91	2.58	0.35	0.08	1.48	2.05									
18	405.36	0.82	1.43	2.95	0.49	0.25	3.49	1.64	18	540.08	0.63	0.98	2.64	0.37	0.10	2.22	2.08	18	561.40	0.69	0.86	3.00	0.29	0.06	1.56	3.64									
19	460.01	0.99	1.63	1.91	0.85	0.57	5.61	1.62	19	515.20	0.63	1.09	3.41	0.32	0.09	1.85	2.01	19	407.45	0.65	1.11	2.47	0.45	0.09	1.65	2.31									
20	563.84	1.14	2.28	2.44	0.94	1.14	9.73	1.69	20	349.09	0.60	0.87	1.83	0.47	0.10	1.65	1.05	20	517.27	0.52	0.74	2.24	0.33	0.06	1.36	3.18									
21	477.51	0.75	1.31	2.58	0.51	0.22	3.06	2.65	21	412.86	0.52	1.35	2.97	0.46	0.14	2.25	3.05	21	475.78	0.53	0.81	2.28	0.36	0.06	1.60	2.59									
22	462.03	1.12	1.55	2.22	0.70	0.40	4.61	2.02	22	396.31	0.83	0.99	2.26	0.44	0.15	2.43	1.83	22	319.02	0.52	0.77	2.25	0.34	0.06	1.53	2.20									
23	432.60	0.98	1.50	2.74	0.55	0.32	4.31	2.01	23	367.25	0.56	0.82	2.12	0.39	0.08	1.77	1.59	23	481.84	0.59	1.04	3.29	0.32	0.08	1.71	2.71									
24	357.91	0.85	1.20	3.06	0.39	0.20	2.73	1.41	24	429.60	0.77	1.01	1.68	0.60	0.21	2.92	1.47	24	350.41	0.61	0.89	3.10	0.29	0.07	1.55	2.11									
25	562.97	0.59	1.11	2.70	0.41	0.10	1.97	2.38	25	562.97	0.59	1.11	2.70	0.41	0.10	1.97	2.38	25	596.59	0.48	0.96	2.85	0.34	0.05	1.56	3.40									
26	316.08	0.70	1.05	2.86	0.37	0.12	2.10	1.60	26	316.08	0.70	1.05	2.86	0.37	0.12	2.10	1.60	26	450.70	0.57	0.92	4.28	0.21	0.05	1.73	4.76									
27	384.79	0.74	0.99	1.96	0.50	0.14	2.37	1.31	27	384.79	0.74	0.99	1.96	0.50	0.14	2.37	1.31	27	529.13	0.59	0.71	2.37	0.30	0.06	1.51	2.79									
28	444.77	0.59	0.77	1.90	0.41	0.07	2.34	2.07	28	444.77	0.59	0.77	1.90	0.41	0.07	2.34	2.07	28	377.64	0.70	1.05	2.66	0.40	0.09	2.22	2.23									
29	533.87	0.60	1.34	4.36	0.31	0.11	2.90	3.63	29	533.87	0.60	1.34	4.36	0.31	0.11	2.90	3.63	29	629.11	0.69	0.88	2.97	0.30	0.07	2.08	5.63									
30	436.57	0.63	0.82	1.66	0.49	0.10	1.75	1.52	30	436.57	0.63	0.82	1.66	0.49	0.10	1.75	1.52	30	465.94	0.63	1.05	4.21	0.25	0.06	1.55	3.89									
31	415.22	0.59	0.98	4.45	0.22	0.05	1.37	2.01	31	415.22	0.59	0.98	4.45	0.22	0.05	1.37	2.01	31	562.33	0.56	0.74	2.30	0.32	0.06	1.53	3.06									
32	283.32	0.51	0.83	2.26	0.37	0.06	1.46	1.87	32	283.32	0.51	0.83	2.26	0.37	0.06	1.46	1.87	32	643.43	0.58	0.84	2.34	0.36	0.06	1.57	5.41									
33	359.44	0.58	1.00	2.23	0.45	0.12	1.93	1.40	33	359.44	0.58	1.00	2.23	0.45	0.12	1.93	1.40	33	452.45	0.57	0.80	2.64	0.30	0.05	1.33	2.47									
34	450.86	0.60	0.88	2.58	0.34	0.06	1.69	1.85	34	450.86	0.60	0.88	2.58	0.34	0.06	1.69	1.85	34	348.68	0.48	0.95	3.33	0.29	0.05	1.27	2.57									
35	440.00	0.62	0.90	2.01	0.45	0.09	1.70	1.68	35	440.00	0.62	0.90	2.01	0.45	0.09	1.70	1.68	35	473.28	0.60	0.72	1.69	0.43	0.06	1.55	2.29									
36	455.89	0.56	0.86	1.95	0.44	0.09	1.61	1.78	36	455.89	0.56	0.86	1.95	0.44	0.09	1.61	1.78	36	443.42	0.50	0.83	4.17	0.20	0.04	1.17	3.41									
37	262.50	0.75	0.94	2.98	0.32	0.09	1.78	1.39	37	262.50	0.75	0.94	2.98	0.32	0.09	1.78	1.39	37																	
38	347.86	0.70	0.88	1.93	0.46	0.09	1.62	1.30	38	347.86	0.70	0.88	1.93	0.46	0.09	1.62	1.30	38																	
39	409.30	0.66	0.91	2.24	0.40	0.10	1.79	1.83	39	409.30	0.66	0.91	2.24	0.40	0.10	1.79	1.83	39																	
40	405.93	0.57	0.86	1.91	0.45	0.10	2.64	1.83	40	405.93	0.57	0.86	1.91	0.45	0.10	2.64	1.83	40																	
41	367.40	0.58	0.82	2.03	0.40	0.07	2.31	1.58	41	367.40	0.58	0.82	2.03	0.40	0.07	2.31	1.58	41																	



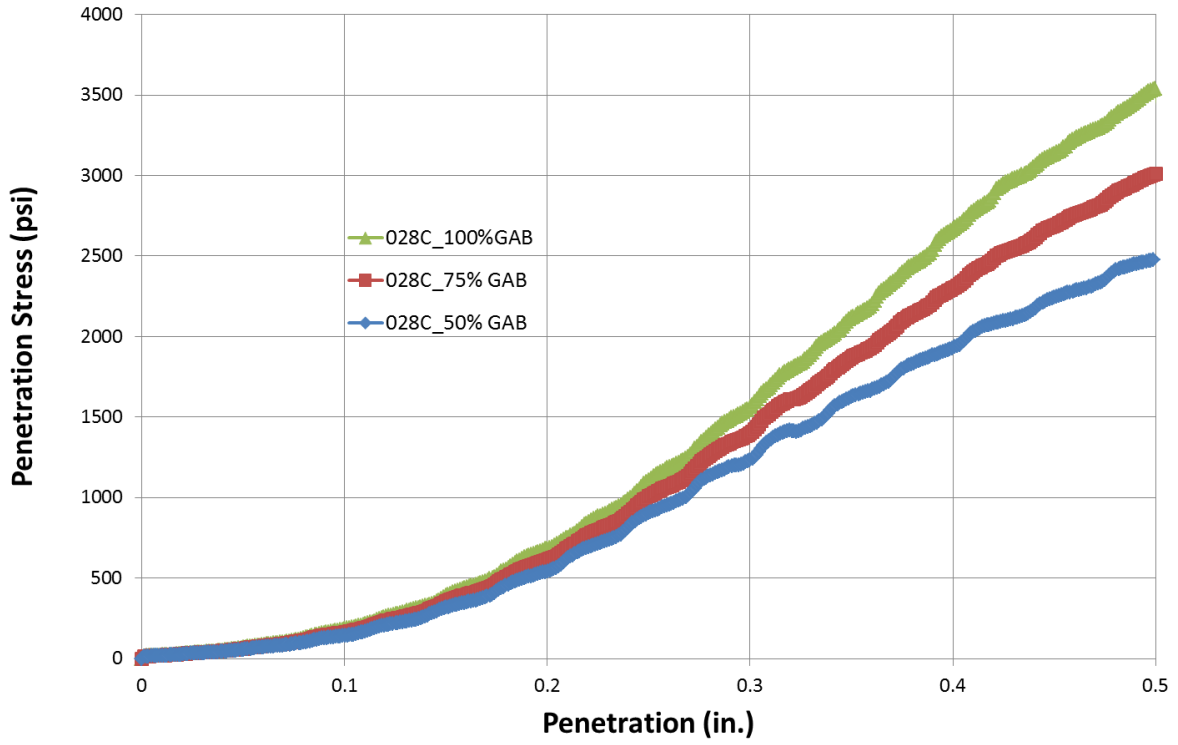
Max	563.8	1.56	2.28	4.34	0.94	1.33	10.88	3.08	Max	562.97	0.91	1.68	4.45	0.60	0.21	3.98	3.63	Max	690.39	0.84	1.33	5.27	0.56	0.14	2.92	5.63
Min	322.8	0.73	1.18	1.58	0.35	0.18	2.73	1.15	Min	262.50	0.51	0.77	1.66	0.22	0.05	1.34	1.05	Min	310.15	0.48	0.71	1.56	0.20	0.04	1.17	1.45
Avg	421.1	1.03	1.60	2.79	0.61	0.44	5.10	1.77	Avg	418.40	0.67	1.04	2.64	0.41	0.12	2.22	1.91	Avg	465.27	0.63	0.94	2.82	0.35	0.08	1.79	2.81
COV	15.4	17.93	19.71	25.32	26.25	62.83	38.04	24.01	COV	16.32	15.33	19.18	27.79	18.30	33.71	25.66	28.42	COV	19.82	14.26	16.40	29.30	24.49	31.19	22.30	34.13

APPENDIX B
CBR Results

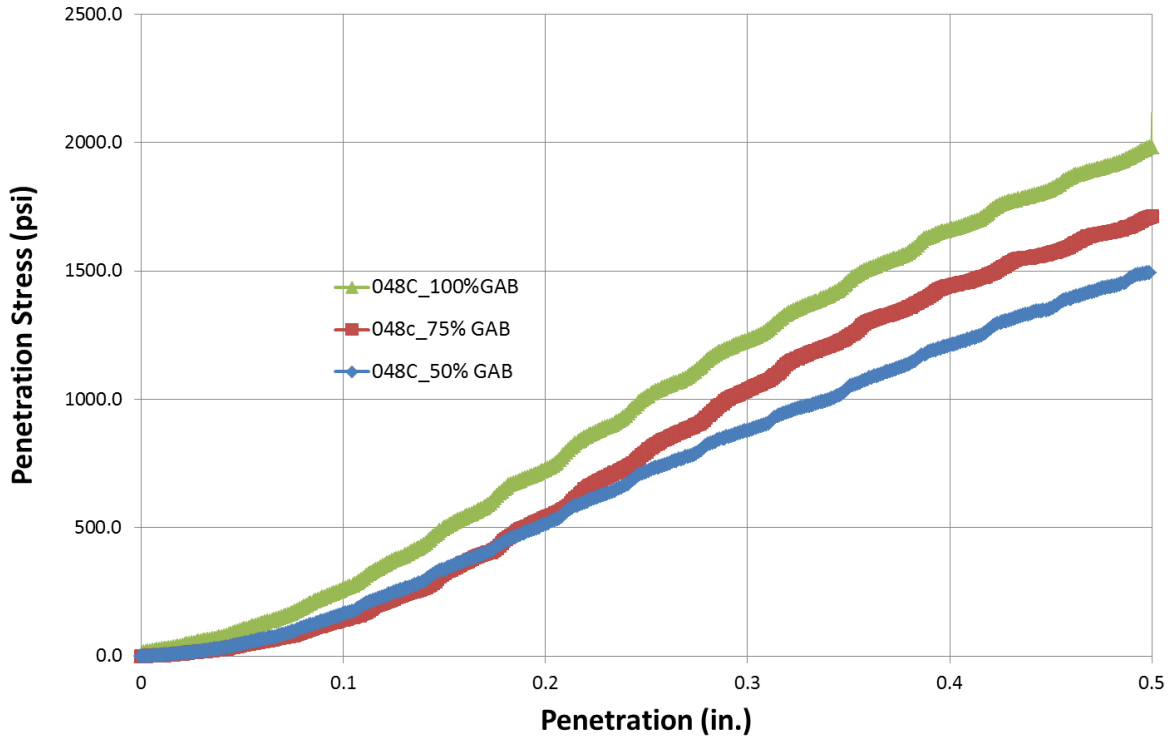
CBR Results (013C)



CBR Results (028C)



CBR Results (048C)



CBR Results (158C)

